# Order-frequency analysis of machine signals

D. Abboud, J. Antoni

Mechanical Systems and Signal Processing 87 (2017) 229–258

Contents lists available at ScienceDirect

Mechanical Systems and Signal Processing

journal homepage: www.elsevier.com/locate/ymssp

# Order-frequency analysis of machine signals

D. Abboud*, J. Antoni

*Laboratoire Vibrations Acoustique, Univ Lyon, INSA-Lyon, LVA EA677, F-69621 Villeurbanne, France*

ARTICLE INFO

*Keywords:*
Order-frequency analysis
Angle/time cyclostationary
Rotating machines
Variable speed conditions
Order-frequency spectral correlation
Improved envelope spectrum

ABSTRACT

Latest researches have asserted the eligibility of angle/time cyclostationarity in analyzing machine signals when operating under variable speed conditions. A core descriptor in this framework is the order-frequency spectral correlation (OFSC), basically estimated by the *averaged cyclic periodogram* (ACP), being able to jointly decode (i) the angle-dependent modulations related to the machine kinematics and (ii) the time-dependent carriers related to the machine dynamics. The present paper comes into this context with the aim of enriching this framework with new tools excerpted from cyclostationarity. In particular, a new estimator of the OFSC based on the *cyclic modulation spectrum* (CMS) is proposed and compared with the ACP in terms of resolution, statistical performance and computational cost. In addition, two related tools are theoretically addressed and their estimators are derived through the ACP and CMS. Specifically, the optimality of the "order-frequency spectral coherence" (the normalized/whitened form of the OFSC) in revealing cyclic components according to their SNR is demonstrated. Also, the "improved envelope spectrum" is derived from the latter by integrating over the spectral frequency variable, evidencing considerable enhancement over the squared envelope spectrum. The potentiality of the proposed tools and the adequacy of the related estimators are experimentally investigated on simulated and real-world vibration signals.

## 1. Introduction

The theory of cyclostationary (CS) processes has proven its efficiency in many fields of science such as meteorology, biology, economy, telecommunication and mechanics [13]. Thanks to this theory, the last two decades have particularly witnessed spectacular progresses in signal processing of machine signals [20]. Specifically, many CS-based techniques have been proposed to deal with various mechanical problems such as machine diagnostics [12,58], system identification [6] and source separation [1–3]. In this context, cyclic spectral analysis is a core discipline of cyclostationarity. It particularly concerns (second-order) CS signals and offers a set of useful tools to analyze them [23]. Being based on the covariance function, the robustness of these tools follows from the consideration of the information redundancy across the cycles (as opposed to the approaches based on local stationarity), thus making it suitable to reveal weak cyclic signatures even when embedded in strong stationary noise [11].

The *spectral correlation* (SC)— originally proposed by Gardner in Ref. [8]— is one of the most efficient tools to detect CS patterns in stochastic signals. It is defined as the double Fourier transform of the covariance function. It is therefore a bi-variable map of two

*Abbreviations:* CS, cyclostationary; SC, spectral correlation; SES, squared envelope spectrum; ACP, averaged cyclic periodogram; CMS, cyclic modulation spectrum; AT-CS, angle/time cyclostationary; OFACP, order-frequency averaged cyclic periodogram; OFCMS, order-frequency cyclic modulation spectrum; OFSCoh, order-frequency spectral coherence; IES, improved envelope spectrum; OFACCoh, order-frequency averaged cyclic coherence; OFCMCoh, order-frequency cyclic modulation coherence; ATCF, angle/time covariance function; TF-IPS, time/frequency instantaneous power spectrum; AF-IPS, angle/frequency instantaneous power spectrum; OLA, overlap add; FBS, filterbank summation; DFT, discrete Fourier transform; FFT, Fast Fourier transform

* Corresponding author.
*E-mail addresses:* d-abboud@live.com, dany.abboud@insa-lyon.fr (D. Abboud), Jerome.antoni@insa-lyon.fr (J. Antoni).

http://dx.doi.org/10.1016/j.ymssp.2016.10.024
Received 20 June 2016; Received in revised form 9 September 2016; Accepted 22 October 2016
Available online 07 November 2016

**Nomenclature**

*Operators*

| | |
|---|---|
| $\mathcal{F}\{*\}$ | Fourier transform |
| $\mathbb{E}\{*\}$ | Ensemble average |
| $\|\|g\|\|^2$ | Energy of $g$ |
| $\otimes$ | Numerical circular convolution |
| $F_{LIP}(h)$ | Time reversed function of $h$ |
| $COT_{\Delta t\to\Delta\theta}\{*\}$ | Computed order tracking transform |
| $DFT^{L}_{n\to k}\{*\}$ | Discrete Fourier transform over the length $L$ |

*Theoretical variables*

| | |
|---|---|
| $t$ | Time variable |
| $\tau$ | Time-lag variable |
| $\theta$ | Angle variable |
| $f$ | Spectral frequency variable |
| $\alpha$ | Cyclic order variable |
| $\omega$ | Angular speed |
| $W$ | Time duration of the realization |
| $\Phi$ | Angular sector spanned during the realization |

*Theoretical quantities*

| | |
|---|---|
| $\mathrm{R}_{2X}(\tau, t)$ | Instantaneous autocorrelation function of $X$ |
| $\mathfrak{R}_{2X}(\tau, \theta)$ | Angle/time autocorrelation function of $X$ |
| $\mathfrak{R}^{\beta}_{2X}(\tau)$ | (Angle/time) cyclic correlation function of $X$ associated with the order $\beta$ |
| $S_{2X}(f;t)$ | Time-frequency instantaneous power spectrum of $X$ |
| $\mathcal{S}_{2X}(f;\theta)$ | Angle-frequency instantaneous power spectrum of $X$ |
| $\mathcal{S}^{\beta}_{2X}(f)$ | Order-frequency cyclic power spectrum of $X$ associated with the order $\beta$ |
| $\mathcal{S}_{2X}(f;\alpha)$ | Order-frequency spectral correlation of $X$ |
| $\gamma_{2X}(f;\alpha)$ | Order-frequency spectral coherence of $X$ |
| $I_{2X}(\alpha)$ | Improved envelope spectrum of $X$ |
| $S_{YZ}(f)$ | Cross-power spectral density of signals $Y$ and $Z$ |

*Estimation variables*

| | |
|---|---|
| $t_n$ | Discrete time variable |
| $n$ | Time index |
| $L_t$ | Digital length of the time signal |
| $\Delta_t$ | Sampling period |
| $\Delta_f$ | DFT resolution of the full length signal |
| $\Delta t$ | Time resolution of the spectrogram |
| $\Delta f$ | Spectral frequency resolution |
| $\Delta\alpha$ | Cyclic order resolution |
| $t'_s$ | Discrete time variable of the spectrogram (decimated) |
| $f_k$ | Discrete spectral frequency variable of the estimators |
| $\alpha_i$ | Discrete cyclic order variable of the estimators |
| $S$ | Number of shifting operations |
| $S_\theta$ | Digital length of the angle-frequency spectrogram over the angle-variable |
| $\theta[n]$ | Angular profile |
| $\omega[n]$ | Angular speed profile |
| $\overline{\omega}$ | Mean speed in the record |
| $\omega_{min}$ | Minimal speed in the record |
| $\omega_{eq}$ | Equivalent speed in the record |
| $\rho$ | Mean to minimal speed in the record |
| $\omega_{max}$ | Maximal speed in the record |
| $h[n]$ | Tapering data-window |
| $N_h$ | Tapering data-window length |
| $W_h$ | Main-lobe effective bandwidth in bins |
| $R$ | Hop size |
| $\xi_Q$ | Variance reduction factor |

*Estimators*

| | |
|---|---|
| $\hat{\mathcal{S}}^{(ACP)}_{2X,L_t}(f_k;\alpha_i)$ | Order-frequency averaged cyclic periodogram of $X$ over a $L_t$-long record |
| $\hat{\mathcal{S}}^{(CMS)}_{2X,L_t}(f_k;\alpha_i)$ | Order-frequency cyclic modulation spectrum of $X$ over a $L_t$-long record |
| $\hat{S}^{(Welch)}_{YZ,L_t}(f_k)$ | Welch estimator of the cross-power spectrum of signals $Y$ and $Z$ over a $L_t$-long record |
| $\hat{S}_{2X,L_t}(t'_s, f_k)$ | Time-frequency spectrogram of $X$ over a $L_t$-long record |
| $\hat{\mathcal{S}}_{2X,L_t}(\theta_m, f_k)$ | Angle-frequency spectrogram of $X$ over a $L_t$-long record |
| $\hat{\gamma}^{(ACP)}_{2X,L_t}(f_k;\alpha_i)$ | Order-frequency averaged cyclic coherence of $X$ over a $L_t$-long record |
| $\hat{\gamma}^{(CMS)}_{2X,L_t}(f_k;\alpha_i)$ | Order-frequency cyclic modulation coherence of $X$ over a $L_t$-long record |
| $\hat{I}^{(ACP)}_{2X,L_t}$ | ACP-based estimator of the improved envelope spectrum of $X$ over a $L_t$-long record |
| $\hat{I}^{(CMS)}_{2X,L_t}$ | CMS-based estimator of the improved envelope spectrum of $X$ over a $L_t$-long record |

frequency variables with different physical meanings, namely the *spectral frequency* and the *cyclic frequency*. The former describes the properties of the stationary carrier on which the cyclic information is traveling, while the latter describes the periodic hidden modulations in the signal. When applied to CS signals, the SC embodies a symptomatic distribution of spectral lines parallel to the spectral frequency axis and located at the modulation cyclic frequencies. The intensity of these lines varies continuously along the spectral frequency axis according to the power spectral density of the carrier. Interestingly, the relationship between the SC and the squared envelope spectrum (SES) has been established in Ref. [18] wherein the SES was proven to equal the integration/summation of the SC over the spectral frequency axis. Viewed differently, when read as a function of the cyclic frequency, the SC of a signal at a given spectral frequency equals the SES applied to the same signal narrowly band-pass filtered at the same frequency. Since then, the SES has been considered as a CS tool [14,24].

The estimation of the SC follows the classical lines of stationary spectral analysis and, particularly, those concerned with the estimation of the power spectrum. A primitive and simple estimator is the (cyclic) periodogram, known to be asymptotically inconsistent and, thus, disregarded in the literature. Similarly to the stationary case, the consistency of the estimator is practically ensured by two methods. The first one inserts a smoothing window in the calculation of the (cyclic) periodogram itself— e.g.

smoothed (cyclic) periodogram, Daniell's estimator, etc. [9,10]. The second one averages short-time (cyclic) periodograms after potential weighting— e.g. averaged (cyclic) periodogram [7]. Outside these two families, the Bartlett's estimator [4] and the multipater (cyclic) periodogram [5] also guarantee the consistency, but they are less popular due to their complexity. Ref. [23] has found that all the aforementioned estimators of the SC (and possibly others) can be devised from a general quadratic form characterized by a smoothing kernel. This form has noticeably served in deriving general expressions for the statistical properties of the estimators (i.e. bias and variance). It has been proven that (consistent) estimators are all asymptotically equivalent and their quality is defined through a common *variance reduction ratio*. Since then, the *averaged cyclic periodogram* (ACP) has become the most popular estimator of the SC in engineering applications benefiting from its low computational cost, principally powered by the fast Fourier transform (FFT) algorithm involved in its calculation. However, the low computational cost of the ACP remains relative (with respect to other existing estimators) since its algorithm is generally expensive. Indeed, the ACP algorithm consists of the calculation of a (cross-) averaged spectrum (i.e. the Welch estimator) for each scanned cyclic frequency, whose number is generally high due to the fine scrutinization needed to unambiguously reveal the discrete cyclic content in the signal.

Away from cyclostationarity, another frequency-frequency distribution— called the *modulation spectrum*— has been used in the speech processing field [16]. It consists of systematically computing the envelope spectrum along multiple frequency bands (carriers). The primary advantage of this quantity is to provide a detailed description about (i) the speaker location and/or environment via the spectral frequency (denoted in the specific literature as the *acoustic frequency*) and (ii) the linguistic information via the cyclic frequency (denoted as the *modulation frequency*) [17]. Often, the modulation spectrum is processed to enhance the signal-to-noise ratio (SNR) and, consequently, enhance speech intelligibility. Later, the modulation spectrum has been revisited in Ref. [20] and addressed within the CS framework in a more general context. First, a comprehensive definition has been assigned to the so-called *cyclic modulation spectrum* (CMS), being the Fourier transform of the spectrogram. Second, its relationship with the SES has been theoretically addressed and intuitively explained. Third, its relationship with the SC has been also established and a brief comparison of these quantities has been performed. Fourth, the CMS efficiency has been successfully tested on real mechanical signals for the first time. Afterwards, a more detailed study of the CMS has been provided in the context of surface ship detection [37]. Recently, the CMS has been formalized in Ref. [47] within the general quadratic form of SC estimators [24]. An unbiased version of the CMS, namely the *envelope-based cyclic periodogram*, has been equally proposed. Remarkably, the formalization of the CMS through the general quadratic form has allowed a deep investigation of its statistical properties, providing another way to understand the *uncertainty principle* that faces such a tool. In particular, it has been shown that the CMS bias dramatically grows beyond a certain cyclic frequency upper limit— called as the *cutoff cyclic frequency*— that depends on the spectral frequency resolution, thus restricting the analysis. Also, a quantitative investigation of the computational cost of the ACP and CMS has been made showing an obvious superiority of the latter over the former.

As advocated in Antoni [58], the capacity of the CS framework in describing machine signals is confined to the stationary regime case— i.e. when the operating speed is constant or stationary. Otherwise, cyclostationarity is jeopardized and its tools (including the SC) turn unreliable no matter whether the signal is processed in time or in angle [22]. Often, rotating machines witness a repetitive occurrence of short-time events being related to its regular operation (such as combustion, piston slap, etc.) or to a certain dysfunction (e.g. a local fault). These events are likely to produce transient signatures whose properties are related to the system dynamics. These transients are time-invariant as they are typically dictated by time-differential equations. However, the recurrence of the events (and the transients) is due to the rotating motions of machine components. It is thus dependent on the machine kinematics and its evolution is inherently locked with the machine rotational angle. It is the presence of this (angle/time) duality that makes rotating machine signals unsuitable to be analyzed within the CS framework in variable speed conditions. Primary solutions for this issue were proposed in D'Elia [59] wherein the authors replaced the frequency-frequency approach by an order-frequency approach. The aim was to jointly describe the angle-periodicities through the order variable and the time-dynamics through the frequency variable. They have proposed two intuitive order-frequency estimators, namely the *α-synchronized spectral correlation density* and *α-synchronized cyclic modulation spectrum*, which respectively extend the SC and CMS to the variable speed case. Later, a fast version of the former estimator, called *speed correlation*, has been proposed in Roussel [60], being based on the speed transform. But, the proposed solution was confined to runup regimes (i.e. constant acceleration). Very recently, a similar definition of the α-synchronized cyclic modulation spectrum was proposed and published in [53] under the name "angular temporal spectrum", yet with a different algorithm.

Recently, the ambiguity of the angle/time duality has been finally unveiled in Refs. [19,21] by setting up the foundations of a new class of *angle/time cyclostationary* (AT-CS) signals; providing a rigorous formalism for machine signal analysis in variable speed conditions. These references have specifically presented three main theoretical findings. First, the angle/time covariance function (ATCF) has been proposed to replace the regular covariance function. This has opened the door to the formalization of the so-called *order frequency spectral correlation* (OFSC), being the double Fourier transform of the ATCF. Also, its normalized form, namely the *order-frequency spectral coherence* (OFSCoh), has been derived. Second, an ACP-based estimator of the OFSC is proposed, having the same computational cost as the speed correlation, yet being free of the linear speed restriction. Third, the statistical properties of this estimator have been studied, offering the possibility to detect AT-CS component through a statistical hypothesis test. Note that, in case of severe speed variations, vibration signals are likely to undergo significant structural changes causing also substantial changes in the signal statistics (e.g. long-term energy and phase modulations, evolution of the signal-to-noise ratio, etc.) [50,51,56,57]. These changes may be induced by the passage of critical speeds, changes in the machine power intake, gyroscopic effects, nonlinearity of the system and other phenomena. In such conditions, these signals turn cyclo-non-stationary [52,59], yet they still hold the AT-CS property on average [21,22]. Recently, Urbanek et al. [53] proposed a normalization step to get rid of the long-term amplitude modulation. This technique could be used as a preprocessing step before an AT-CS analysis.

These latest advances have left the door open to enrich the AT-CS framework with new tools. In particular, this paper formally addresses the extension of the CMS within the AT-CS framework. The obtained quantity, namely the *order-frequency cyclic modulation spectrum* (OFCMS), is considered as an estimator of the OFSC. This estimator is compared with the previously adopted *order-frequency averaged cyclic periodogram* (OFACP) in terms of resolution, statistical performance and computational cost. Some useful tools will be equally derived and their estimation is proposed.

The paper is organized as follows: Section 2 provides a comprehensive view of machine signals through the AT-CS framework, giving a special attention on their description by means of the OFSC. Section 3 addresses the estimation issue of the OFSC by first reviewing the OFACP and, then, proposing the OFCMS. A comparison of them in terms of resolution, statistical performance and computation cost is provided with some guidelines for parameter settings. Section 4 derives related quantities, namely the *order frequency spectral coherence* (OFSCoh) and the *improved envelope spectrum* (IES), and discusses their estimations. Section 5 validates the theoretical findings in two numerical experiments and two real applications in various case studies. Finally, the paper is sealed with a general conclusion in section 6.

## 2. Order-frequency description of machine signals

The object of this section is to provide a comprehensive view of machine signals through the AT-CS framework. For this purpose, an overview of the AT-CS class is first provided together with its main dedicated tools. The distinctive properties of these tools on AT-CS signals are analyzed, given a special attention on how to decode such signals in the order-frequency plane.

### 2.1. Rotating machine signals

In rotating machines, a succession of events is likely to occur within the machine cycle so that the released energy varies on a rhythmic basis. These events are likely to produce transient signatures in vibration signals which, in turn, carry critical information on the machine health [20]. Interestingly, the concept of *diagnostic information* is jointly related to (i) the periodicity of the events and (ii) the properties of the transients, thus their identification is of high interest for machine diagnostics. The occurrence of these events is related to the machine kinematics, thus its periodicity is consistent in the angle domain [26]. On the contrary, transients are mostly generated by physical phenomena typically described by time-dependent dynamical characteristics, thus their properties are consistent in the time domain. The vibration signal emitted by a local fault in a REB is perhaps the most representable example. In details, REB vibrations consist of a series of cyclic impacts phase-locked to the shaft angle and exciting structural resonances [22]. Clearly, the positions of the impact excitations are dictated by the shaft angle while the resonance responses are governed by temporal differential equations that impose time-invariant properties (e.g. natural frequencies and relaxation times). Therefore, the periodicity of the impacts is consistent in angle, while the properties of the impulse response hold in time. It is the presence of this (angle/time) duality that makes rotating machine signals unsuitable to be analyzed within the CS framework in variable speed conditions (i.e. when the angle/time relationship is strongly nonlinear). In consequence, the reputed efficiency of CS tools is jeopardized in this case . From here was the need for a wider framework able to analyze speed-varying signals. Next subsections review and discuss a solution for this issue based on a *joint* angle/time vision.

### 2.2. Angle/time cyclostationary signals

The theory of AT-CS signals was originally introduced in Ref. [19] with the purpose of modeling random rotating machine signals in variable speed conditions. According to this theory, AT-CS signals are found to be the product between angle-periodic modulations and time-stationary carriers. Stated differently, an AT-CS signal (e.g. a rotating machine signal), $X(t)$, can be modeled through a Fourier series whose basis functions, $e^{\mathrm{j}k\theta}$, are expressed in the angle-domain and whose Fourier coefficients, $\mathrm{c}_X^k(t)$, are mutually time-stationary random processes, viz

$$X(t) = \sum_{\beta\in\mathbb{Z}} \mathrm{c}_X^{\beta}(t) e^{\mathrm{j}\beta\theta(t)}, \tag{1}$$

where $t$ and $\theta$ are respectively the time and angle variables, and it has been assumed that a full cycle corresponds to $2\pi$ radians, $\beta$ is the cyclic orders, $\mathrm{c}_X^{\beta}$ is the Fourier coefficient of $X$ associated with the cyclic order $\beta$ and $\mathbb{Z}$ is the set of integers which also (and without loss of generality[1]) designs the *cyclic order set*. In general, angle and time are interrelated by the following equation:

$$\theta(t) = \int_0^t \omega(\mathrm{t})dt, \tag{2}$$

where $\omega(\mathrm{t})$ denotes the instantaneous angular speed (in radians/s). The AT-CS phenomenon is illustrated in Fig. 1(a).

To decode AT-CS signals, a *joint* consideration of the angle and time variables is needed. For this purpose, the "angle/time

[1] The signal $X(t)$— as defined in Eq. (1)— refers to a strict AT-CS signal. The concept may easily be extended to the case of *poly-* and *quasi-* AT-CS signals by changing the cyclic order set just like in the cyclostationary case [58].

autocorrelation function" (ATCF) was proposed as

$$\mathfrak{R}_{2X}(\tau,\ \theta)=\mathbb{E}\{X(t(\theta))X(t(\theta)-\tau)^*\}=R_{2X}(\tau,\ t(\theta)) \tag{3}$$

where $\tau$ denotes the time-lag variable, $\mathbb{E}$ is the ensemble averaging operator and $R_{2X}(\tau, t)$ is the regular *instantaneous autocorrelation function* [25]. The above equation states that the ATCF is effectively the instantaneous autocorrelation function at the time instant $t(\theta)$ locked with the angular position $\theta$. Hence, it measures the temporal autocorrelation of the carrier through the time-lag $\tau$ at the angular position $\theta$. This slight adjustment has a significant effect in machine signal analysis as the ATCF turns periodic for AT-CS signals and thus accepts Fourier series with non-zero Fourier coefficients at the cyclic orders,

$$\mathfrak{R}_{2X}(\tau,\ \theta)=\sum_{\beta\in\mathbb{Z}}\mathfrak{R}^{\beta}_{2X}(\tau)e^{j\beta\theta}, \tag{4}$$

where $\mathfrak{R}^{\beta}_{2X}(\tau)$ is the *angle/time cyclic correlation function* (the proof can be found in Appendix A). This aspect is illustrated in

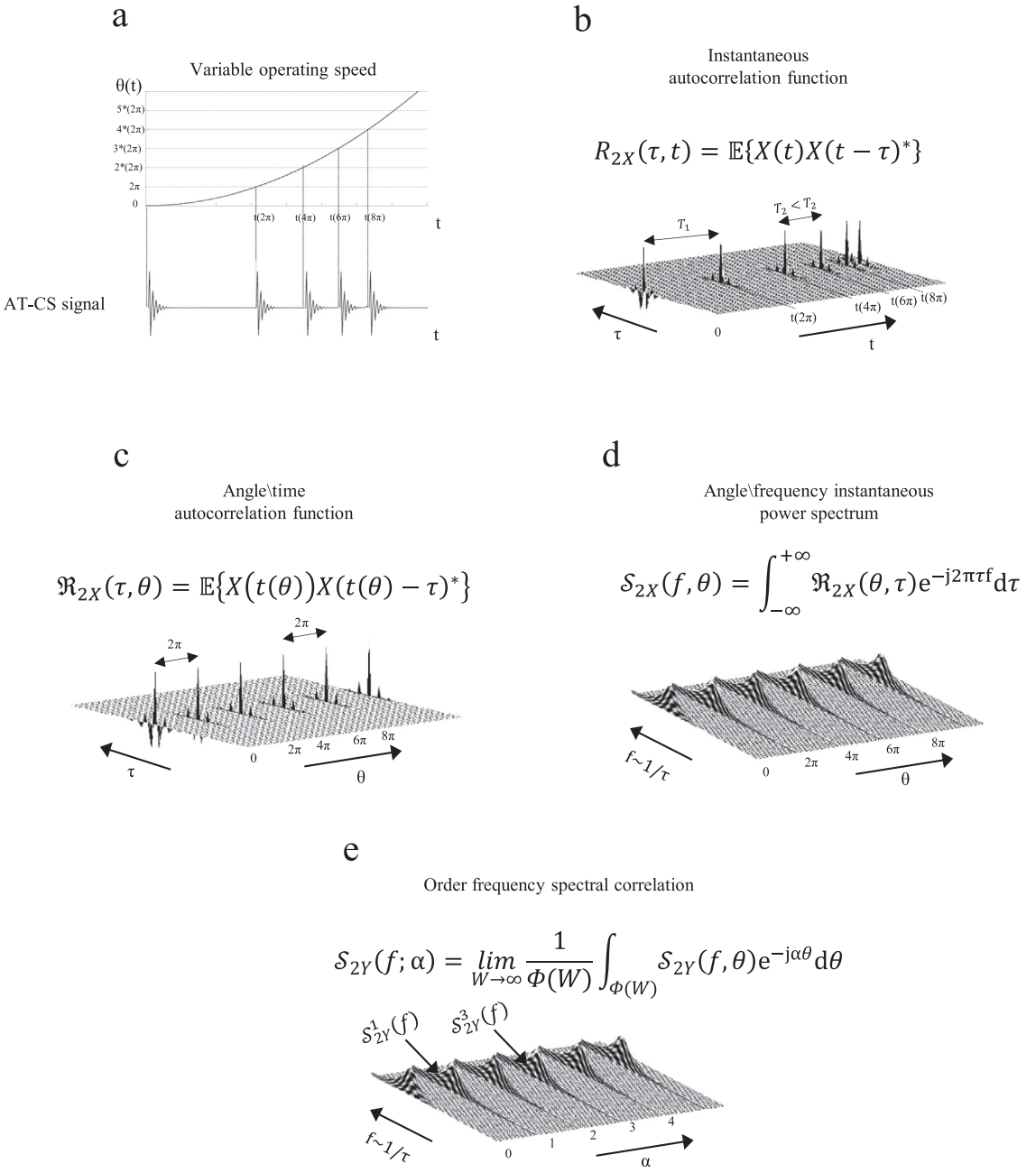


**Fig. 1.** Academic example illustrating: (a) the AT-CS phenomenon, (b) the instantaneous autocorrelation function, (c) the ATCF, (d) the AF-IPS and (e) the OFSC.

Fig. 1(b) and (c). Interestingly, the Fourier decomposition in Eq. (4) fully describes the signal properties: it separates the ATCF into two sets of functions with different physical meanings, namely the Fourier coefficients $\mathfrak{R}_{2X}^{\beta}(\tau)$ and the exponential kernels $e^{j\beta\theta}$. On a hand, $\mathfrak{R}_{2X}^{\beta}(\tau)$ exclusively depends on the time-lag and describes the (second-order) statistical properties of the time-stationary carriers. On the other hand, $e^{j\beta\theta}$ exclusively depends on the angular variable and reflects the cyclic flow of the waveform. Surely, a more prominent way to describe an AT-CS signal is by investigating its spectral statistics. The next subsection deals with this issue.

### 2.3. Spectral properties

As indicated in Ref. [19], the ATCF is a core statistics from which other specialized tools can be devised. Among these tools, the "angle-frequency instantaneous power spectrum" (AF-IPS) can be defined by applying the Fourier transform to the ATCF with respect to the time lag, viz

$$\mathcal{S}_{2X}(f,\ \theta) = \int_{-\infty}^{+\infty} \mathfrak{R}_{2X}(\theta,\ \tau)\mathrm{e}^{-\mathrm{j}2\pi\tau f}\mathrm{d}\tau = S_{2X}(f,\ t(\theta)) \tag{5}$$

where $S_{2X}(f,\ t)$ denotes the *time-frequency instantaneous power spectrum* (TF-IPS) [25]. Similarly to the ATCF, the AF-IPS can be seen as the instantaneous power spectrum at the instant $t(\theta)$ locked with the angular position $\theta$. Last, it is worth noting that the AF-IPS is a power density of unit [$\mathrm{U}^2$/Hz] (where [U] is the unit of $X(t)$— e.g. [$\mathrm{m/s}^2$] for a vibration signal).

For AT-CS signal, the AF-IPS is angle-periodic and accepts a Fourier series

$$\mathcal{S}_{2X}(f,\ \theta) = \sum_{\beta\in\mathbb{Z}} \mathcal{S}_{2X}^{\beta}(f)e^{j\beta\theta} \tag{6}$$

with non-zero Fourier coefficients $\mathcal{S}_{2X}^{\beta}(f)$ *exclusively* associated with the signal cyclic orders $\beta$. The AF-IPS of an AT-CS signal is illustrated in Fig. 1(d). These non-zero coefficients are henceforth called the *order-frequency cyclic power spectra*[2] of unit [$\mathrm{U}^2$/Hz]. It is noteworthy that, as shown in appendix A, $\mathcal{S}_{2X}^{\beta}(f)$ is actually the sum of the cross-power spectra between the coefficient $\mathrm{c}_X^{\beta}(t)$ and all the coefficients (including $\mathrm{c}_X^{\beta}(t)$ itself). Since these coefficients are jointly stationary, the distribution $\mathcal{S}_{2X}^{\beta}(f)$ is expected to be continuous along the $f$-axis and to describe the spectral properties of the carrier. This remarkable property will permit to conceive an order-frequency quantity able to detect and identify angle/time cyclostationarity in random signals.

### 2.4. Order-frequency description

In order to characterize the angle/time cyclostationarity of a random signal, say $Y(t)$, at a given order, say $\alpha$, one has to check the presence of a non-zero Fourier coefficient of the AF-IPS at that order. As a result, one may define the *order-frequency spectral correlation* (OFSC) as the *Fourier coefficient* of the AF-IPS,

$$\mathcal{S}_{2Y}(f;\alpha) = \lim_{W\to\infty} \frac{1}{\Phi(W)} \int_{\Phi(W)} \mathcal{S}_{2Y}(f,\ \theta)\mathrm{e}^{-j\alpha\theta}\mathrm{d}\theta, \tag{7}$$

where $\Phi(W) = \int_W \omega(t)dt$ is the angular sector spanned during the signal time duration $W$. Similarly to the AF-IPS, the OFSC is a power density of unit [$\mathrm{U}^2$/Hz]. It was shown in Ref. [21] that Eq. (7) is equivalent to

$$\mathcal{S}_{2Y}(f;\alpha) = \lim_{W\to\infty} \frac{1}{\Phi(W)} \mathbb{E}\{\mathcal{F}_{t\to f}^{\mathrm{W}}\{Y(t)\}^{*}\mathcal{F}_{t\to f}^{\mathrm{W}}\{Y(t)e^{-\mathrm{j}\alpha\theta}\omega(t)\}\}, \tag{8}$$

where $\mathcal{F}_{t\to f}^{\mathrm{W}}\{Z(t)\} = \int_{-\mathrm{W}/2}^{+\mathrm{W}/2} Z(t)\mathrm{e}^{-\mathrm{j}2\pi\mathrm{t}f}\mathrm{dt}$ denotes the Fourier transform of signal $Z(t)$ over a time interval of finite duration $W$. This expression provides another interpretation of the OFSC, which actually justifies its name: it is a measure of the spectral correlation of the signal itself $Y(t)$ and of its transformed version $Y_{\alpha}(t)=Y(t)e^{-\mathrm{j}\alpha\theta(t)}\omega(t)W/\Phi(W)$ at the spectral frequency $f$. To be more precise, one can reformulate Eq. (8) as:

$$\mathcal{S}_{2Y}(f;\alpha) = S_{YY_{\alpha}}(f), \tag{9}$$

where $S_{YZ}(f) = \lim_{W\to\infty} W^{-1}\mathbb{E}\{\mathcal{F}_{t\to f}^{\mathrm{W}}\{Y(t)\}^{*}\mathcal{F}_{t\to f}^{\mathrm{W}}\{Z(t)\}\}$ denotes the cross-power spectral density of signals $Y$ and $Z$. Without getting into details, the line at $\alpha = 0$ returns an image of the regular power spectrum (in [$\mathrm{U}^2$/Hz]) of the signal

$$\mathcal{S}_{2Y}(f;0) = \mathcal{S}_{2Y}^{0}(f) \sim S_{2Y}(f), \tag{10}$$

where perfect equality only holds for constant speed profile. Evidently, this case describes the stationary behavior of the signal; thus it will be henceforth disregarded.

For AT-CS signals (i.e. $Y(t)=X(t)$ ), the OFSC has the following characteristics:

[2] This designation is excerpted from the *cyclic power spectrum* defined for CS signals and extensively studied in Ref. (Antoni 2007).

$$\mathcal{S}_{2X}(f;\alpha)=\begin{cases} S_{2X}(f) for \alpha=0 \\ \mathcal{S}^{\beta}_{2X}(f) for \alpha=\beta\in\mathbb{Z}^* \\ 0 elsewhere. \end{cases} \tag{11}$$

The OFSC of an AT-CS signal is illustrated in Fig. 1(e). In words, the OFSC is a bi-dimensional map constituted from a collection of continuous parallel lines discretely distributed over the α-axis at the cyclic orders $\beta\in\mathbb{Z}^*$. This symptomatic distribution is what makes the OFSC efficient to detect and identify AT-CS components associated with distinctive mechanical signatures.

## 3. The order-frequency spectral correlation in practice

This section investigates the practical issues of estimating the OFSC. It starts by reviewing a well-known estimator based on the ACP and proposing another one based on the CMS. These estimators are then compared in terms of resolution, statistical performance and computation cost. Based on these comparisons, some guidelines are eventually proposed to properly set the estimation parameters.

### 3.1. Presentation of the estimators

This paragraph is dedicated to presenting two estimators for the OFSC. It initially starts by defining the common notations between the estimators, before reviewing an ACP-based estimator and proposing an CMS-based estimator.

*3.1.1. General notations.* Let $\{X(t_n)\}_{n=0}^{L_t-1}$ be a finite-length record having a nonstationary speed profile $\{\omega(t_n)\}_{n=0}^{L_t-1}\omega(n)$, where $t_n=n\Delta_t$ refers to time instants acquired with sampling period $\Delta_t$. Whenever convenient, any stream of samples, say $Y(t_n)$, will be simply noted $Y[n]$. The speed profile is assumed to be arbitrary varying between $\omega_{min}$ and $\omega_{max}$, with a mean frequency $\overline{\omega}=\sum_{n=0}^{L_T-1}\omega[n]/L_T$. The angular position is related to the speed through the equation: $\theta[n]=\Delta_t\sum_{m=0}^{n-1}\omega[m]$, so the angular length of the signal is $\theta[L_T]=\overline{\omega}L_T\Delta_t$.

Also, the concept of *overlapping windows* is used in both estimators, thus $h[n]=\{h(t_n)\}_{n=0}^{N_h-1}$ will henceforth denote $\{w[n]\}_{n=0}^{N_w-1}$a tapering data-window of $N_h$ $N_w$points having an energy $||h||^2=\sum_{n=0}^{N_h-1}|h[n]|^2$ . Let $h_s[n]=h[n-sR]w_s[n]=w[n-sR]$ be its shifted version by the hop size $R$ $(0<R\leq N_h)$. The quantity $(N_h-R)/N_h\in[0,1[$ is to be interpreted as the overlap rate. The number of shifting operations will be denoted by $S$ which equals the greatest integer smaller than or equal to $(L_t-N_h)/R+1$.

Regarding the estimator variables, the discrete spectral frequency axis will be denoted by $f_k=k\Delta f$ and the discrete cyclic order axis will be denoted by $\alpha_i=i\Delta\alpha$ ($k$ and $i$ are integers), where $\Delta f$ and $\Delta\alpha$ are respectively the spectral frequency and cyclic order resolutions.

*3.1.2. The order-frequency averaged cyclic periodogram (OFACP).* As indicated in Ref. [19], Eq. (8) offers the possibility to estimate the OFSC with classical estimators dedicated to the SC. Among various estimators, the averaged cyclic periodogram (ACP)[3] is perhaps the most practical because of its easy implementation, and its relatively low computational cost as compared to other existing *bilinear* estimators[4] (e.g. smoothed cyclic periodogram) while maintaining optimal asymptotic properties [23]. Up to now, it is the only used estimator for the estimation of the OFSC [21,22,27]. This estimator, henceforth called the *order-frequency averaged cyclic periodogram* (OFACP), can be defined in a compact way by means of the Welch estimator of the cross-power spectrum [21],

$$\hat{\mathcal{S}}^{(ACP)}_{2X,L_t}(f_k;\alpha_i)=\hat{S}^{(Welch)}_{XX_{\alpha_i},L_t}(f_k), \tag{12}$$

where $X_{\alpha_i}[n]=X[n]e^{-j\alpha_i\theta[n]}\omega[n]/\overline{\omega}$ and $\hat{S}^{(Welch)}_{YZ,L_t}(f_k)$ is the Welch estimator of the cross-power spectrum of signals $Y[n]$ and $Z[n]$ over a $L_t$-long record [32],

$$\hat{S}^{(Welch)}_{YZ,L_t}(f_k)=\frac{\Delta_t}{L_tS\|h\|^2}\sum_{s=0}^{S-1}DFT^{N_h}_{n\to k}\{h_s[n]Y[n]\}^*DFT^{N_h}_{n\to k}\{h_s[n]Z[n]\}, \tag{13}$$

where $DFT^{N_h}_{n\to k}\{Y[n]\}=\sum_{n=0}^{N_h-1}Y[n]e^{-j2\pi(n\Delta_t)(k\Delta f)}$ is the discrete Fourier transform (DFT) over $N_h$ samples. Readers can find the related MATLAB routine in Ref. [21].

*3.1.3. The order-frequency cyclic modulation spectrum (OFCMS).* The idea of designing an order-frequency distribution from the CMS is not new. In fact, it has been addressed in a previous contribution (D'Elia, 2010). This subsection reconsiders its extension within the AT-CS framework and proves its optimality with respect to the previous one. Just like the CMS, the newly proposed

[3] Also referred as the Welch-based estimator.
[4] The term 'bilinear' refers to the nonlinear quadratic transform involved in the computation of these estimators [33].

estimator is based on the spectrogram. For this purpose, a brief comprehensive review of the spectrogram is first displayed and two related algorithms are investigated. Next, the CMS-based estimator of the OFSC is proposed. Last, a comparison between the latter and the one proposed in Ref. [59] is provided.

*3.1.3.1. Prerequisite: estimation of the TF-IPS.* The *spectrogram* is the most common estimator of the TF-IPS. It consists of computing the power spectrum on small and possibly overlapped sections of the signal:

$$\hat{S}_{2X,L_t}(f_k;t_s') = \frac{\Delta_t}{L_t\|h\|^2}\left|DFT_{n\to k}^{N_h}\{h_s[n]X[n]\}\right|^2. \tag{14}$$

Eq. (14) can be equivalently rewritten as

$$\hat{S}_{2X,L_t}(f_k;t_s') = \frac{\Delta_t}{L_t\|h\|^2}|X(t_{sR};f_k)|^2, \tag{15}$$

with

$$X(f_k;t_n) = Y[n]\otimes \check{h}[n;f_k] = \sum_{r=0}^{N_h-1}\check{h}[r;f_k]Y[n-r] \tag{16}$$

($\otimes$ denotes the *numerical convolution*) and $\check{h}[n;f_k] = \check{h}[n]e^{-j2\pi n\Delta_t f_k}$ ($\check{h} = F_{LIP}(h)$ is the time reversed window) to be interpreted as a bandpass filter of central frequency $f_k$ and a bandwidth $\Delta f$. At this stage, it is worth noting that the discrete time axis is decimated by $R$ i.e. $\hat{S}_{2X,L_t}(t_s', f_k) = \hat{S}_{2X,L_t}(t_{sR}, f_k)$ with $t_s'=s\Delta t$ and $\Delta t = R\Delta_t$. On the other hand, the frequency axis is implicitly decimated by a factor $S$: $f_k=k\Delta f = kS\Delta_f$ (with $\Delta_f = 1/(L\Delta_t)$ the DFT resolution of the full length signal). Surely, this decimation reduces the information redundancy and, hence, can prevent unnecessary memory allocation when implementing this tool.

Despite their mathematical equivalence, Eqs. (14) and (15) provide different physical interpretations and algorithmic implementations of the estimator. Whereas the former is interpreted as the *local* power spectrum of the signal at the time instants $t_s' = t_{sR}$, the latter is interpreted as the squared envelopes of the output of a filterbank (whose central frequencies are located at $f_k$) and down-sampled by a ratio $R$. In fact, one is the Fourier dual of the other [55]. These interpretations provide two algorithms to implement the estimator known in the literature as the *overlap add (OLA)* (Eq. (14) and *filterbank summation (FBS)* methods (Eq. (15)) [35,55].

Regarding its computational cost, the OLA algorithm requires $S$ DFT operation over $N_h$-long window for all the time instants $t_{sR}$. Assuming that the FFT is used ($N_h$ is a power of two) and $S\sim L_t/N_h$, the OLA algorithm cost scales almost as:

$$C_{OLA}\sim L_t\log_2 N_h. \tag{17}$$

On the other hand, the FBS algorithm requires a circular convolution for each spectral frequency $f_k$; thus its cost scales almost as $O(R.L_T\log_2 L_T)$ for the *standard circular convolution* method,[5] but can be more efficiently computed by means of the *overlap add decomposition* method[6] [31,29]. In the latter case, the leading term in the overall FBS algorithm complexity is:

$$C_{FBS}\sim\frac{L_tN_h}{(N_{seg}-N_h+1)}N_{seg}\log_2 N_{seg}\sim N_hL_t\log_2 N_{seg} \tag{18}$$

where $N_{seg}$ denotes the length of the segment used for the decomposition and should be chosen as: $N_h \ll N_{seg} \ll L_T$ [34]. As a result, the OLA algorithm is computationally more efficient than the FBS with a gain in the computational cost equivalent to

$$\frac{C_{FBS}}{C_{OLA}}\sim\frac{N_h\log_2 N_{seg}}{\log_2 N_h}\sim N_h\log_{N_h}N_{seg}\sim O(N_h) \tag{19}$$

where $\log_{N_h}N_{seg}$ is the logarithm of $N_{seg}$ in base $N_h$. The above equation is clear: the OLA algorithm is at least $N_h$ times faster than the FBS algorithm ($\log_{N_h}N_{seg}>1$). For this reason, the former will be henceforth adopted for the estimation of the TF-IPS.

*3.1.3.2. Definition.* The extension of the CMS to the variable speed case directly follows from Eq. (7). This gives birth to a new estimator, henceforth called the *order-frequency cyclic modulation spectrum* (OFCMS), which equals the Fourier transform of the angle/frequency spectrogram (i.e. which is the spectrogram-based estimator of the AF-IPS). This latter is simply obtained by order tracking the spectrogram with respect to the time variable, i.e.

$$\hat{S}_{2X,L_t}(f_k;\theta_m) = COT_{\Delta t\to\Delta\theta}\{\hat{S}_{2X,L_t}(f_k;t_s')\} \tag{20}$$

where $\theta_m=m\Delta\theta$ and $COT_{\Delta t\to\Delta\theta}\{*\}$ is the *computed order tracking* transform which resamples a signal— originally sampled with constant-time increment $\Delta t$— at constant angular increments spaced by $\Delta\theta$ [26,45]. This can be simply made through an interpolation provided that an accurate measure of the angular position exists (e.g. a tachometer signal). To avoid aliasing, the

[5] The standard circular convolution method requires two DFT operations over the full signal length.

[6] In signal processing, the overlap–add decomposition method is an efficient way to evaluate the discrete convolution of a very long signal with a finite impulse response filter. The concept is to divide the problem into multiple convolutions of the filter with short segments of the signal. The computational cost of these short-segment convolutions by the FFT algorithm is less than the convolution of the full-length signal.

angular increment must be chosen to respect the inequality $\Delta\theta \leq \omega_{min}\Delta t = \omega_{min} R \Delta_t$ [28] (again, $\omega_{min}$ denotes the minimum speed in [rad/s]) of the machine in the record. The obtained angle-frequency distribution is an $S_\theta$-by-$N_h$ matrix where $S_\theta = \theta[L_T]/\Delta\theta$. In order to decrease the computational cost, it is recommended to choose: $\Delta\theta = \omega_{min}\Delta t$. In this case, the numerical length along the angular variable is: $S_\theta = \rho . S$, where $\rho = \overline{\omega}/\omega_{min}$ is the ratio between the mean and the minimal speeds.

Afterwards, the OFCMS is obtained by Fourier transforming the AF-IPS estimate with respect to the angle:

$$\hat{S}^{(CMS)}_{2X,L_t}(f_k;\alpha_i) = \frac{1}{S_\theta} DFT^{S_\theta}_{m\to i}\{\hat{S}_{2X}(\theta_m;f_k)\} \tag{21}$$

where $DFT^{S_\theta}_{m\to i}\{Y[m]\} = \sum_{m=0}^{S_\theta-1} Y[m] e^{-j(i\Delta\alpha)(m\Delta\theta)}$. Readers will find the related Matlab routine in Appendix B.

Last but not least, it is beneficial to point out the physical interpretation of $\hat{S}^{(CMS)}_{2X,L_t}(f_k,\ \alpha_i)$. When seen as a function of $\alpha_i$, the OFCMS returns for each spectral frequency at $f_k$, the squared envelope spectrum of the bandpass filtered signal at the same frequency with a bandwidth $\Delta f$. On the other side, when seen as a function of $f_k$, it returns the cyclic power spectrum for each cyclic frequency $\alpha_i$.

Eventually, it is noteworthy that the COT operation (Eq. (20)) followed by the DFT (Eq. (21)) can be replaced by the *velocity synchronous discrete Fourier transform*:, a transform proposed in Ref. [44] which maps a discrete-time signal to its discrete order-domain counterpart. At first glance, such transform seems more appropriate as it directly maps the time-frequency spectrogram to the OFCMS. However, as stated in the same reference, this transform turns to become computationally very expensive (as compared with the COT+DFT) when the number of scanned cyclic orders is high. Since the perfect knowledge of the signal cyclic order set is not usually available even after a kinematic study (e.g. deviation of characteristic orders in REBs, varying number of harmonics and sidebands, etc.), a scrutinization of relatively high number of cyclic orders is typically required. This explains why this strategy was not adopted when defining the OFCMS.

*3.1.3.3. Discussion about previous works.* As previously pointed out, D'Elia [59] were the first who explore the need of an order-frequency analysis for a prominent description of REB vibrations in variable speed. The so-called *α-synchronized cyclic modulation spectrum* was proposed as an extension of the CMS. They propose an order tracking operation at the output of a digital filterbank, before squaring and Fourier transformation. Undoubtedly, their algorithm resembles the proposed OFCMS and may return identical results if the parameters are suitably chosen. However, it inherently imposes the use of the FBS algorithm for spectrogram calculation which, according to Section 3.2.1, unnecessarily increases the computational cost of the quantity. Moreover, the authors have not mentioned any recommendation about the choice of the filterbank central frequencies and bandwidth. If these latter were carelessly chosen, this would either bias the estimator and impoverish its frequency precision (e.g. if $\Delta f \gg 1/(\Delta_t N_h)$) or unnecessarily increase its computational cost (e.g. if $\Delta f \ll 1/(\Delta_t N_h)$). Into addition, no decimation step was proposed by the authors at the output of the filterbank. Aside from being memory consuming, this will again increase the computational time of the algorithm as (i) the interpolated points in the order tracking operation will increase $R$ times and, eventually, (ii) the last (angle-to-order) DFT operation will be applied to longer signals.

Recently, the "angular temporal spectrum" was proposed in [54] in the same manner as the α-synchronized cyclic modulation spectrum, but with a different algorithm which is closer to the one proposed in this paper. Conversely, the present one defines the OFCMS as an estimator of the OFSC, thus formalizing it within the AT-CS framework. This connection was firstly explored in Ref. [47] for the stationary speed case (in the CS framework), and is now extended to the variable speed case (in the AT-CS framework). For all these reasons, the authors believe that the OFCMS— as defined in the present paper— is the straightforward way to generalize the CMS to the variable speed case.

### 3.2. Comparison between estimators

This paragraph compares the OFACP and OFCMS on the basis of their (i) resolution, (ii) statistical performance and (iii) computational cost. A discussion is eventually provided to reveal their mutual influences.

*3.2.1. Frequency resolutions.* Provided that the window type, the window length, the hop size and the signal length are the same, the OFACP and OFCMS share similar frequency resolution along the $\alpha$-axis as well as the $f$-axis. These resolutions are briefly investigated hereafter.

*3.2.1.1. Cyclic order resolution $\Delta\alpha$.* The cyclic order resolution of both estimators equals the inverse of the number of cycles executed by the reference angle, i.e.

$$\Delta\alpha = \frac{2\pi}{\theta[L_T]} = \frac{2\pi}{\overline{\omega} L_T \Delta_t} \tag{22}$$

Contrary to constant speed case (i.e. for ACP and CMS) [47], this resolution is not only dependent on the signal length $L_T$, but also on the record mean speed $\overline{\omega}$. Indeed, for a fixed record length, the cyclic resolution gets coarser for low mean speeds and vice-versa.

*3.2.1.2. Spectral frequency resolution $\Delta f$.* The spectral frequency resolution of both estimators equals the spectral bandwidth of the tapering window function, viz

$$\Delta f = W_h \frac{1}{(N_h - R)\Delta_t} \sim \frac{1}{N_h \Delta_t}. \tag{23}$$

where $W_h = N_h \|h\|^2 / (\sum_{n=0}^{N_h-1} h[n])^2 \geq 1$ is the main-lobe *effective bandwidth* in bins [41] (for instance, $W_h$=1 with a rectangular window, $W_h$=1.4 with a Hamming/Hanning window and $W_h$=1.2 for a half sine window [40].

*3.2.2. Statistical performance.* The bias and variance analysis of the ACP and CMS have been thoroughly studied in Refs. [23,37,47]. The aim of this paragraph is to extend these results to the variable speed case. For the OFCMS, it will be assumed hereafter that the data-window length $N_h$ (i) is longer than the correlation length of the signal and (ii) shorter than the speed variability (i.e. $\omega[n] \approx \omega[n+m]$ for all $n$ and $0 < m \leq N_h$).

*3.2.2.1. Bias analysis.* For large $L_t$, the OFACP is an unbiased estimator:

$$\mathbb{E}\left\{\hat{\mathcal{S}}_{2X,L_t}^{(ACP)}(f_k;\alpha_i)\right\} \approx \mathcal{S}_{2X}(f_k;\alpha_i), \tag{24}$$

provided that an important overlap rate is set. Practically, setting $R > N_h/3$ with a Hanning/Hamming data-window or $R > N_h/2$ with a half-sine data-window achieves excellent bias cancellation[7] [23].

On the other hand, the OFCMS is asymptotically biased,

$$\mathbb{E}\left\{\hat{\mathcal{S}}_{2X,L_t}^{(CMS)}(f_k;\alpha_i)\right\} \approx \mathcal{S}_{2X}(f_k;\alpha_i) \frac{\overline{\mathcal{S}}_{2h}(\alpha_i)}{\overline{\mathcal{S}}_{2h}(0)}, \tag{25}$$

with

$$\overline{\mathcal{S}}_{2h}(\alpha_i) = \frac{1}{S} \sum_{p=0}^{S-1} \left(\frac{\omega[pR]}{\overline{\omega}}\right) S_{2h}(2\pi\alpha_i \omega[pR]) \tag{26}$$

where $S_{2h}(f)$ denotes the power spectrum of $h$. Since $S_{2h}(f)$ is a bandpass filter of effective bandwidth $\Delta f/2$, $\overline{\mathcal{S}}_{2h}(\alpha_i)$ then consists of a *weighted sum* of bandpass filters with speed-dependent order-bandwidth equal to $\pi\Delta f/\omega$: the higher the speed is, the narrower the order bandwidths are. Since the sum is weighted by the speed, it thus favors high-speed order filters. Consequently, $\overline{\mathcal{S}}_{2h}(\alpha_i)/\overline{\mathcal{S}}_{2h}(0)$ can be fairly approximated by an order-domain low pass filter of unit gain with a (3 dB) *cutoff cyclic order*: $\alpha_{cut} = \pi\Delta f/\omega_{eq}$ (where $\omega_{eq}$ is the equivalent speed: $\omega_{eq} = \|\omega\|^2/L_t\overline{\omega}$ and $\|\omega\|^2 = \sum_{n=0}^{L_t-1} \omega[n]^2$). Return to Eq. (25), the OFCMS is only able to estimate the OFSC within the filter bandwidth, i.e. for

$$\alpha_i \leq \alpha_{cut} = \frac{\pi\Delta f}{\omega_{eq}} = \frac{\pi\Delta f \overline{\omega}}{\|\omega\|^2}. \tag{27}$$

Viewed differently, the fact that the highest cyclic order seen by the OFCMS is bounded upward by $\alpha_{cut}$ is a direct consequence of the uncertainty principle in the variable speed case [20], $T_{min}\Delta f/2 \geq 1$ with $T_{min} = 2\pi/(\alpha_i\omega_{eq})$, which basically affects the spectrogram: modulations which are faster than allowed by the frequency resolution are not detected. Note that a condition similar to Eq. (27) was previously found in Ref. [36], but with the use of maximal speed $\omega_{max}$ instead of the equivalent speed $\omega_{eq}$. Such a condition is actually too conservative as it imposes that the modulation associated with $\alpha_{cut}$ must never exceed the filter bandwidth— i.e. $\alpha_{cut}\omega[n]/2\pi < \Delta f/2$ for all $n$. In the most of practical applications, the use of $\omega_{eq}$ is justified as modulations in the signal can still be identified.

Eventually, Eq. (25) offers the opportunity to define an unbiased version of the OFCMS with proper calibration (similarly to the envelope-based cyclic periodogram [47]. Yet, such step would complicate its computation without enhancing the estimator variance (more on the subject is addressed in the next subsection).

*3.2.2.2. Variance analysis.* The general form of an OFSC estimator variance reads:

$$Var\{\hat{\mathcal{S}}_{2X,L_t}(f_k;\alpha_i)\} \approx \xi_Q(\alpha_i) S_{2X}(f_k) S_{2X_{\alpha_i}}(f_k) \tag{28}$$

where $\xi_Q(\alpha_i)$ is the variance reduction factor.

As indicated in Ref. [22], the variance reduction factor of the OFACP equals that of the regular ACP, i.e. [23]

$$\xi_Q^{(ACP)} = \sum_{s=0}^{S-1} \frac{R_{2h}[sR]^2}{\|h\|^4} \frac{S-|s|}{S^2} \sim O(N_h/L_t), \tag{29}$$

[7] This bias manifests as a cyclic leakage along the cyclic order axis.

where $R_{2h}[n]$ is the autocorrelation function of the data-window $h[n]$. Despite its simplicity, Eq. (29) carries fundamental information on the estimation properties as well as the influential parameters. First, $\xi_{\mathrm{Q}}^{(ACP)}$ is constant implying a uniform variance reduction in the $(f;\alpha)$ plane. Second, $\xi_{\mathrm{Q}}^{(ACP)}$ is a decreasing function of the number of averages $S$; it begins with unity when no averaging is made (i.e. $S=1$)[8] and it gradually decreases when $S$ increases. Therefore, the OFACP variance converges to zero for large $L_t$. Since $\xi_{\mathrm{Q}}^{(ACP)}$ is a decreasing function of $L_t/N_h$, the latter ratio will dictate the estimation quality. Last, the overlap rate plays an important role in decreasing the variance as $\xi_{\mathrm{Q}}^{(ACP)}$ is a decreasing function of $R/N_h$. In practice, setting $R>N_h/3$ for classical data-windows (e.g. Hanning, Hamming, half-sine) will return minimal variance reduction [23].

For the OFCMS, proceeding with the calculation reported in Ref. [47], the variance reduction factor reads

$$\xi_{\mathrm{Q}}^{(CMS)}(\alpha_i)=\frac{\sum_{k=-S/2+1}^{S/2}\left|\overline{\mathcal{S}}_{2h}(f_k;\alpha_i)\right|^2}{\left|\sum_{k=-S/2+1}^{S/2}\overline{\mathcal{S}}_{2h}(f_k;\alpha_i)\right|^2}, \tag{30}$$

where

$$\overline{\mathcal{S}}_{2h}(f_k;\alpha_i)=H^*[f_k].\left(\frac{1}{S}\sum_{p=0}^{S-1}\frac{\omega[pR]}{\overline{\omega}}H[f_k+2\pi\alpha_i\omega[pR]]\right) \tag{31}$$

and $H[f]$ stands for the frequency response function of $h[n]$ and $f$. As explained in Ref. [47][9], $\xi_{\mathrm{Q}}^{(CMS)}(\alpha_i)$ is an increasing function of $\alpha_i$ which converges to zero as the signal length grows towards infinity for $\alpha_i<\alpha_{cut}$. Its flatness is however dictated by the data-window type: a smooth data-window (e.g. Gaussian, half-sine, Hamming/Hanning, etc.) can guarantee a flat variance over the $\alpha_i$-axis. By approximating the data-window by a Gaussian window, one may simplify Eq. (30) to [47]:

$$\xi_{\mathrm{Q}}^{(CMS)}(\alpha_i)\approx\frac{\mathrm{N_h}}{\sqrt{\pi}L_t}\sim O(\mathrm{N_h}/L_t)\,for\,\alpha_i<\alpha_{cut}. \tag{32}$$

In conclusion, the OFCMS shares similar statistical properties as the OFACP for $\alpha_i<\alpha_{cut}$ though being slightly biased. Above $\alpha_{cut}$, the estimation error (i.e. bias and variance) significantly increases and the returned values get noisy and inaccurate: this is another way to understand the uncertainty principal that limits the OFCMS. The estimation quality of both estimators is dictated by $L_t/\mathrm{N_h}$: the higher the ratio is, the better the estimation is.

*3.2.3. Computational cost.* The evaluation of the OFACP at $M$ cyclic orders requires $M$ computations of the Welch estimator of the cross-spectrum which, in turn, needs to compute $2S$ times DFT over $N_h$-data points. Assuming that the FFT is used ($N_h$ is a power of two) and $S\sim L_t/N_h$, the leading term in the overall OFACP complexity is

$$C_{ACP}\sim ML_t\log_2 N_h. \tag{33}$$

On the other hand, the computational cost of the OFCMS starts with the calculation of the spectrogram. This involves the DFT of $S$ blocks of data-length$N_h$, thus needing $S$ $N_h$-point FFTs for computation. Then, the order tracked spectrogram is Fourier transformed in the angle direction $N_h$-times, needing the computation of $S_\theta$-point FFTs. Ignoring other computations (such as the interpolation in Eq. (20)), the leading term in the overall complexity is

$$C_{CMS}\sim SN_h\log_2 N_h+N_hS_\theta\log_2 S_\theta\sim\rho L_t\log_2\rho L_t, \tag{34}$$

where, again, $\rho$ is the ratio between the mean and the minimal speeds and $S_\theta=\rho S\sim\rho L_t/N_h$.

For the sake of comparison, the computational cost of the OFACP computed over the same cyclic order in the range $[0,\alpha_{cut}]$ requires $M=\alpha_{cut}/\Delta\alpha$. After some manipulations, the gain in computational cost of the OFCMS with respect to the OFACP simplifies to

$$\frac{C_{CAP}}{C_{CMS}}\sim\left(\frac{\overline{\omega}^3\log_2 N_h}{\omega_{min}||\omega||^2\log_2\rho L_t}\right)\frac{L_t}{N_h}\sim O\left(\frac{L_t}{N_h}\right). \tag{35}$$

Eq. (35) indicates that the computation gain grows proportionally with the ratio $L_t/N_h$ which, according to Section 3.3.2, defines the estimators' quality. Practically, a high $L_t/N_h$ is needed to reduce the estimation errors; therefore the OFCMS is much faster than the OFACP in the general scenario. Last, it is worth noting that the gain is also influenced by the speed profile (note the terms into brackets); though their effect remains secondary as compared with the signal length.

*3.2.4. Discussion.* Regarding the OFACP, the computational cost of this estimator is inversely proportional to the number of the scanned cyclic orders which is, in turn, inversely proportional to the number of cycles in the record. It is asymptotically a consistent estimator having (i) an asymptotically nil bias and (ii) a uniformly distributed variance reduction factor. The variance reduction is a

[8] In this particular case, the estimator is called the "order-frequency cyclic periodogram".

[9] The CMS as defined in this paper (by setting constant $\omega[n]=\omega_0$) is the biased envelope-based cyclic periodogram proposed in Ref. Borghesani ($year$) [47]. In fact, the latter is an algorithm of the former (with proper calibration for bias compensation) principally based on the FBS algorithm involved in the spectrogram calculation.

decreasing function of the temporal duration, but also of the computational cost. Stated differently, the statistical performance of the OFACP is balanced by its computational cost.

On the other hand, the OFCMS estimator is computationally more efficient than the OFACP with a gain linearly growing with the signal length. In details, whether an OLA or FBS algorithm is involved in its computation; the OFCMS inherently— and uniformly— scans the spectral frequencies: its computational cost is mainly related to the scanned frequency bins (which are dictated by the tapering-window length). Recognizing that the order-frequency distribution of an AT-CS signal is expected to be discrete along the $\alpha$-axis and continuous to the $f$ -axis, a fine scrutinization is thus required along the $\alpha$α-axis to not miss out a spectral line, whereas a relatively coarse scrutinization of the $f$f-axis is typically sufficient to reveal the corresponding spectral content. Evidently, the computational cost is lower when scrutinizing the latter; this explains the obvious superiority of the OFCMS in terms of computational cost.

However, the OFCMS is faced by the uncertainty principle which, according to Eq. (27), limits the choice of $\alpha_{cut}$ $\alpha_{\max}$ and $\Delta f$Δf according to the maximal rotating frequency of the reference $\omega_{\max}$$\omega_{\max}$. In practice, the expected cyclic order set produced by the modulations of an arbitrary rotating component is derived based on a prior kinematic study. Thus, if $\Delta f$ is reasonably fixed to detect the spectral content, $\alpha_{cut}$ will be too low to detect the desired cyclic order set for high speeds. On the contrary, if $\alpha_{cut}$ is reasonably fixed to detect the cyclic components of interest, $\Delta f$ is likely to be too coarse to accurately reveal the spectral content of the signal. In the ultimate case, the distribution may boil down to the SES in the case of very high speeds i.e. the complete loss of the spectral content. At any rate and regardless of the signal length, the OFCMS is not able to jointly reveal the order and the frequency content of the signal with high precision. Interestingly, the OFACP is free from these restrictions since it is effectively an (angle/time) density function and, consequently, not limited by the uncertainty principle.[10]

In conclusion, if there is no restriction on the calculation time, the OFACP is undoubtedly the best way to estimate the OFSC. Otherwise, the OFCMS may provide a very-fast alternative. In this case, it is important to check whether $\alpha_{cut}$ $f_{\max}$ is sufficiently moderate to ensure a trade-off between (i) a reasonable $\Delta f$ able to identify the carrier spectral properties Δfand (ii) an $\alpha_{\text{cut}}\alpha_{\max}$ sufficiently larger than the expected cyclic order signature. This explains the excellent compliance of the CMS for surface ships detection from radiated propeller noise (CS signal) in [37]: the generating mechanism (the blades) turns at low speed ensuring both a reasonable spectral resolution and a high cutoff order (or frequency).

### 3.3. Parameter settings

The previous paragraph has discussed the influence of the estimation parameters on the resolution, statistical performance and computational cost. These findings will enable us to propose some guidelines to set the essential estimation parameters, namely the window length $N_h$, the record length $L_t$ and the hop size $R$.

*3.3.1. Setting the window length $N_h$.* As shown in Eq. (23), the window length $N_h$ dictates the spectral resolution for both estimators; thus it should be chosen greater than twice the signal correlation length. While respecting this condition, $N_h$ must be chosen as small as possible in order to decrease (i) the computational cost of the estimators (see Eqs. (33) and (34)), as well as (ii) the variance reduction ratios (see Section 3.2.2.2). Once $N_h$ is set, the spectral resolution $\Delta f$ and, consequently, the cutoff order $\alpha_{cut}$ (see Eq. (27)) are fixed. At this stage, the suitability of the OFCMS can be tested according to the expected cyclic order set of interest. The latter is typically known following an *a priori* study of the system kinematics.[11] The authors recommend the use of the OFCMS only if the expected cyclic order set is lower than $\alpha_{cut}$. In this case only, the OFCMS enjoys satisfying statistical properties.

*3.3.2. Setting the record length $L_t$.* According to Eq. (22), the acquisition length is the main factor which defines the cyclic order resolution, $\Delta\alpha$, of both order-frequency estimators. It is thus essential to detect AT-CS components and $\Delta\alpha$ must be chosen fine enough to not miss out the spectral lines. To do so, one needs to investigate the minimal order spacing, say $\Delta\alpha^{(\min)}$, between the components of the expected cyclic order set and make sure that its value is greater than $\Delta\alpha$. Stated differently, $L_t$ must respect the following inequality

$$L_T > \frac{2\pi}{\overline{\omega}\Delta_t\Delta\alpha^{(\min)}}. \tag{36}$$

In words, the record must be chosen sufficiently large to include enough cycles so that the corresponding cyclic resolution gets fine enough to unambiguously detect the spectral lines. In fact, this condition is essential to protect against the effect of the energy leakage phenomenon along the cyclic order axis. Also, the equation above indicates that the average speed also affects the choice. The

[10] The computation of the OFACP is implicitly based on the angle-frequency Wigner-Ville spectrum, contrary to the OFCMS which is based on the angle-frequency spectrogram.

[11] For instance, to diagnose a REB, one needs to systematically compute the fault frequencies of each suspected element (e.g. outer or inner race fault orders) [38,39].

lower the speed is, the lower the number of executed cycles is, and the larger the record length must be.

Eq. (36) gives the first condition to choose the record length for both estimators, yet another factor should be considered: the estimation quality. In details, according to Eqs. (29) and (32), the variance reduction factor of both estimators are decreasing functions of $L_t/N_h$. Thus, the record length must be chosen much larger than the window length: $L_t \gg N_h$ ($L_t/N_h$ is typically in the order of few tens or hundreds).

Eventually, it is undoubtedly safe to choose $L_t$ sufficiently large to some extent; yet, one should be keen about the consequences in terms of computational cost as the latter may dramatically increase with $L_t$ (see Eqs. (33) and (34)).

*3.3.3. Setting the hop size R.* The hop size should be wisely chosen to optimally exploit existing data while avoiding as musch as possible information redundancy. It mainly depends on the window type as this size systematically decreases with the flatness (in the time domain) of the window. Ideally, the hop size must ensure a tradeoff between (i) the resulting flatness of the *data weighting* and (ii) *overlap correlation*. Data weighting is simply the weight (influence) of each point in the data stream and can be measured by linearly and quadratically[12] summing all window values that are applied to a particular data point [42]. Otherwise, overlap correlation is a measure of information relationship among consecutive stretches and is defined as the ratio of the window autocorrelation function at the hop size and its energy: $R_{2h}[R]/||h||^2$ [40]. Evidently, high overlap correlation results in a waste of computational effort by repeatedly computing highly correlated results.

Ideally, the hop size must be great enough to ensure maximum possible flatness of data weighting, while not unnecessary boosting the computational cost. Readers can find useful recommendation about the optimal overlap for a variety of windows in Ref. [43]. An additional particularity for the CMS-based estimator is the need of a small $R$ to protect against spectral aliasing in the $\alpha$-axis [37]. The authors particularly recommend the use of Hamming/Hanning window which can guarantee perfect flatness of data weighting and a reasonable overlap correlation for $R = 0.25N_h$ (i.e. 75% overlap).

*3.3.4. General methodology.* This section gathers the guidelines discussed in the previous subsections into a step-by-step methodology to set the estimation parameters:

1. Acquire the acceleration signal $x[n]$ and compute the speed profile $\omega[n]$ via the tachometer signal.
2. Perform a kinematic study of the system to define the cyclic order set of interest. An idea about the cutoff order $\alpha_{cut}$ (which should be greater than the maximal order of interest) and the minimal order spacing $\Delta\alpha^{(\min)}$ is obtained.
3. Set the record length $L_T$ with respect to Eq. (36).
4. Define the window (e.g. Hanning), then choose $N_w$ such as to return a reasonable spectral resolution$\Delta f$ (see Eq. (23)) while being ideally a power of two. Then set the overlap rate accordingly (75% is recommended).
5. Evaluate the estimation quality $L_T/N_w$. If the value is not satisfactory, then take a higher $L_T$.
6. Apply the estimators' algorithm.

## 4. Related quantities

Refs. [23,24] have derived useful related tools from the classical SC. Of particular interest are the spectral coherence and the integrated cyclic coherence. This section follows the same concept to derive similar quantities from the OFSC in variable speed.

### 4.1. The order-frequency spectral coherence

#### 4.1.1. Definition

As advocated in Ref. [21], a prominent order-frequency distribution is the (squared-magnitude) "order-frequency spectral coherence" (OFSCoh) which is defined as:

$$\gamma^2_{2Y}(f;\alpha) = \frac{|\mathcal{S}_{2Y}(f;\alpha)|^2}{S_{2Y}(f;0)S_{2Y_\alpha}(f;0)}. \tag{37}$$

The above quantity implicitly includes a whitening/normalizing operation which (i) cancels out the uneven distribution of the signal power in the frequency domain and (ii) bounds its values between 0 and 1. To see this, let's investigate the OFSCoh on the AT-CS signal $X(t)$ given in Section 2; it takes this particular form:

[12] The linear summing of window values checks the amplitude flatness of the data weighting and is particularly appropriate for deterministic signals such as chirps, whereas the quadratic summing checks the amplitude flatness and is appropriate for incoherent or random signals such as noise.

$$\gamma_{2X}^2(f;\alpha) = \begin{cases} 1 for \alpha = 0 \\ \frac{\left|S_{XX_\beta}(f)\right|^2}{S_{XX}(f)S_{X_\beta X_\beta}(f)} for \alpha = \beta \in \mathbb{Z}^* \\ 0 elsewhere \end{cases}$$

$$\sim \begin{cases} 1 for \alpha = 0 \\ SNR_{2X}^\beta(f) for \alpha = \beta \in \mathbb{Z}^* \\ 0 elsewhere \end{cases} \tag{38}$$

where

$$SNR_{2X}^\beta(f) = \left|\frac{\mathcal{S}_{2X}^\beta(f)}{S_{2X}(f)}\right|^2 = \left|\frac{S_{XX_\beta}(f)}{S_{2X}(f)}\right|^2 \tag{39}$$

denotes the (squared-magnitude) signal-to-noise ratio of the AT-CS component associated with the cyclic order $\beta$ (the signal) relative to the stationary component (the noise). According to Schwartz inequality, the latter is smaller than or equal to unity. Therefore, the OFSCoh is expected to return strictly positive real spectral lines parallel to the $f$-axis and located at the cyclic orders associated with the signal cyclic order set.

To summarize, $\gamma_{2X}^2(f;\alpha)$ is a real quantity that returns positive non-zero values lower than unity in the form of parallel lines discretely distributed at the cyclic orders associated with the signal cyclic order set. These lines are continuous and their intensity increases with the SNR, contrary to the OFSC where the magnitude of the spectral lines increases with the carriers power spectrum. For this reason, it is often more efficient to highlight the presence of angle/time cyclostationarity.

### 4.1.2. Estimation

Regarding its estimation, the OFSCoh can be estimated from the OFACP, giving birth to the "order-frequency averaged cyclic coherence" (OFACCoh) defined as:

$$\begin{aligned} \hat{\gamma}_{2X,L_t}^{2(ACP)}(f_k;\alpha_i) &= \frac{\left|\hat{S}_{2X,L_t}^{(ACP)}(f_k;\alpha_i)\right|^2}{\hat{S}_{2X,L_t}^{(ACP)}(f_k;0)\hat{S}_{2X_\alpha,L_t}^{(ACP)}(f_k;0)} \\ &= \frac{\left|\hat{S}_{XX_{\alpha_i},L_t}^{(Welch)}(f_k)\right|^2}{\hat{S}_{2X,L_t}^{(Welch)}(f_k)\hat{S}_{2X_{\alpha_i},L_t}^{(Welch)}(f_k)}. \end{aligned} \tag{40}$$

Also, the OFSCoh can be estimated through the OFCMS, giving birth to the "order-frequency cyclic modulation coherence" (OFCMCoh) defined as:

$$\begin{aligned} \hat{\gamma}_{2X,L_t}^{2(CMS)}(f_k;\alpha_i) &= \frac{\left|\hat{S}_{2X,L_t}^{(CMS)}(f_k;\alpha_i)\right|^2}{\hat{S}_{2X,L_t}^{(CMS)}(f_k;0)\hat{S}_{2X_{\alpha_i},L_t}^{(CMS)}(f_k;0)} \\ &\approx \left|\frac{\hat{S}_{2X,L_t}^{(CMS)}(f_k;\alpha_i)}{\hat{S}_{2X,L_t}^{(CMS)}(f_k;0)}\right|^2. \end{aligned} \tag{41}$$

It is worth noting that the first line of Eq. (41) shares similar (expensive) computational cost as the OFACP since it requires the calculation of the OFCMS (or alternatively the Welch power auto-spectrum) of $X_{\alpha_i}[n]$ for each value $\alpha_i$. But, according to subsection 3.2, the validity of the OFCMS estimator is restricted to low values of $\alpha_i$ so that $\alpha_i\omega[n]/2\pi < \Delta f$ almost for all $n$. Therefore, by reasonably assuming a smooth spectrum of the signal, one may safely accept: $\hat{S}_{2X_{\alpha_i},L_t}^{(CMS)}(f_k;0) \approx \hat{S}_{2X,L_t}^{(CMS)}(f_k;0)$ [37]. Therefore, the second line of Eq. (41) will be adopted when estimating the coherence.

## 4.2. The integrated squared spectral coherence

Most often, vector indicators are preferred in industry as their readability is generally simple and does not require advanced skills in signal processing. Accordingly, one may sacrifice the optimality of the OFSCoh by integrating over the spectral frequency variable preferably in a high SNR frequency band (or simply over the whole frequencies). Precisely, one may devise a suboptimal quantity, henceforth called the "improved envelope spectrum" (IES)—as:

$$I_{2Y}(\alpha) = \frac{1}{F_2 - F_1}\int_{F_1}^{F_2} \gamma_{2Y}^2(f;\alpha)df, \tag{42}$$

where $F_1$ and $F_2$ are respectively the lower and upper bounds of the integration frequency domain. Note that the concept of defining $I_{2Y}(\alpha)$ slightly differs from that of the integrated cyclic coherence [24] as it consists of integration over real positive values

instead of complex values. Therefore, this concept seems more suitable to promote non-zero cyclic components which may average distinctively when integrating complex values in the case of fast rotating phases [48].

For AT-CS signals,

$$I_{2X}(\alpha) = \begin{cases} 1 for \alpha = 0 \\ SNR_{2X}^{\beta;[F_1;F_2]} for \alpha = \beta \in \mathbb{Z}^* \\ 0 elsewhere \end{cases} \tag{43}$$

where

$$SNR_{2X}^{\beta;[F_1;F_2]} = \frac{1}{F_2 - F_1} \int_{F_1}^{F_2} SNR_{2X}^{\beta}(f) df \tag{44}$$

stands for the SNR of the AT-CS component associated with the cyclic order $\beta$ in the spectral frequency band $[F_1; F_2]$ relative to stationarity. It is bounded in [0,1] and returns higher values with the intensity of the AT-CS component in this band. Interestingly, this quantity returns a symptomatic discrete normalized distribution in the presence of AT-CS components, providing significant enhancement over the regular envelope analysis [24,48].

Regarding the estimation, the integral in Eq. (44) will turn into a summation over discrete spectral frequencies regardless of the adopted estimator. Accordingly, the "ACP-based estimator of the IES" (ACP-IES) becomes

$$\hat{I}_{2X,L_t}^{(ACP)} = \frac{1}{K_2 - K_1 + 1} \sum_{K_1}^{K_2} \hat{\gamma}_{2X,L_t}^{2(ACP)}(f_k; \alpha_i), \tag{45}$$

whereas the "CMS-based estimator of the IES" (CMS-IES) becomes

$$\hat{I}_{2X,L_t}^{(CMS)} = \frac{1}{K_2 - K_1 + 1} \sum_{K_1}^{K_2} \hat{\gamma}_{2X,L_t}^{2(CMS)}(f_k; \alpha_i), \tag{46}$$

with $0 \leq K_1 < K_2 < N_h/2$ ($K_1$ and $K_2$ are integers).

## 5. Examples of application

The principal object of this section is to experimentally validate the theoretical findings and the comparisons on simulated and real-world signals. For this purpose, two numerical experiments are first provided. The first one particularly investigates and compares the bias and the computational cost of the OFACP and OFCMS, while the second one evaluates the proposed tools on a simulated AT-CS signal. After that, two real applications are provided to demonstrate the effectiveness of these tools on real vibration signals. The first application investigates the diagnosis of a REB in a simple machine fault simulator, while the second one investigates the diagnosis of a REB in a complex civil aircraft engine.

### 5.1. Numerical experiment 1

The aim of this experiment is to numerically illustrate the bias of OFSC estimators as well as their computational cost. A white noise is thus used to evenly excite all frequencies and orders in the $(f;\alpha)$ plane. The OFACP and OFCMS are applied to a 2 s white noise record of sampling rate equal to 10 kHz with 75% overlapping Hanning window of length $N_h$=128. Fig. 1 exposes the (normalized) mean value obtained over 1000 runs for the four speed profiles: (i) constant speed equal to 20 Hz, (ii) runup from 15 Hz to 20 Hz, (iii) runup from 10 Hz to 20 Hz, (iv) runup from 5 Hz to 20 Hz. First, the mean values of both estimators share the same distribution over the $f$-axis; thus the displayed plots refer to an arbitrary spectral frequency. Second, the OFACP mean value is independent of the corresponding speed profile (which agrees with Eq. (24)); thus only that related to the second speed profile is displayed in the figure. Third, the OFCMS mean value appears as a low pass filter along the $\alpha$-axis whereof its cutoff order depends on the speed profile. This agrees with Eq. (27) in which the cutoff order was shown to depend on the speed profile (specifically the equivalent speed $\omega_{eq}$). In order to evaluate the results, the (3 dB) cutoff orders of the four profiles are theoretically computed by means of Eq. (27) and displayed as four vertical lines in Fig. 1. Interestingly, the intersection of these line with the OFCMS means perfectly coincidences at −3 dB; hence obviously asserting the theoretical findings.

Next, the computational gain of the OFCMS relative to the OFACP (i.e. $C_{CAP}/C_{CMS}$) is computed for profile (ii) for different record lengths and the obtained results averaged over 50 runs are displayed in Fig. 2. The other estimation parameters are maintained as in the previous case. The theoretical gain is also calculated through Eq. (35) and displayed in the same figure for comparison. Both plots witness similar evolution with the ratio $L_t/N_h$ which, according to Section 3.2.2.2, dictates the estimation quality of both estimators. For instance, the OFACP is computationally 100 times more expensive than the OFCMS for a ratio $L_t/N_h$=128 (which is a very common value in practice). Note that the difference between the theoretical and numerical gain is principally due to the neglected operations (specifically the interpolation in the COT) involved in the OFCMS calculation. For this reason, the numerical gain is slightly smaller than the theoretical one and this difference increases with the signal length (since the impact of the neglected operations increases for large $L_t$).

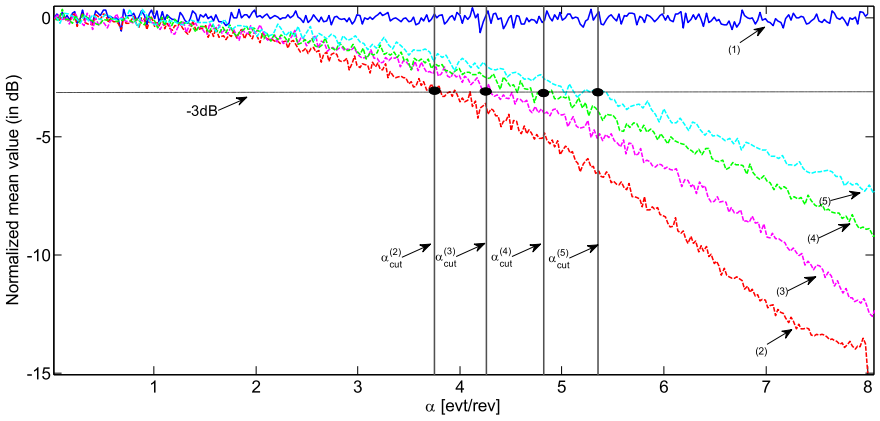


**Fig. 2.** The (normalized) mean value of the OFSC magnitude applied to a white noise with different speed profiles, and obtained with a 1000 run Monte Carlo simulation : (1) OFACP (run-up: 15–20 Hz), (2) OFCMS (constant speed: 20 Hz), (3) OFCMS (run-up: 15–20 Hz) , (4) OFCMS (run-up: 10–20 Hz) , (5) OFCMS (run-up: 5–20 Hz). The vertical lines denote the theoretical (3 dB) cutoff-order of the corresponding OFCMS (the superscript refers to the plot number) calculated with Eq. (27). The intersection of the OFCMS plots (2 to 5) with the −3 dB lines are to be interpreted as the numerical (3 dB) cutoff orders, while the vertical lines are the theoretical ones.

### 5.2. Numerical experiment 2

This experiment investigates the OFSC estimators together with their related tools on an AT-CS signal embedded in stationary noise. The instantaneous frequency (i.e. speed profile) is a runup from 15 Hz to 20 Hz. The sampling frequency is 10 kHz and the record duration is 4 s (i.e. 40 ksamples), which correspond to 70 cycles executed by the reference angle (1 cycle is equivalent to $2\pi$ radians). The AT-CS signal is constructed by multiplying (i) an angle-periodic modulation constituted from the sum of 40 chirps whose instantaneous frequencies are multiple of half of the speed profile (from order 0.5 to 20) with (ii) a Gaussian colored noise (the carrier) of limited frequency-band [3 kHz, 4 kHz]. In turn, the stationary noise is constituted from two signals of equal energy: (i) a Gaussian colored noise of limited frequency-band [1.25 kHz, 1.75 kHz] and (ii) a Gaussian white noise. The noise power equals 18 times the (AT-CS) signal power— i.e. $SNR = -12.5dB$.

Before applying the OFSC estimators, one needs to check whether the signal length is large enough to reveal the cyclic order content of the distribution (see Section 3.3.2— Eq. (36)). As shown in Section 3.2.1.1, the cyclic order resolution equals the inverse of the number of executed cycles: $\Delta\alpha = 1/70 = 0.0143$. Besides, the expected cyclic order set is expected to be multiple of the fundamental order 0.5—i.e. $\beta \in \{0.5k; k = 1, 2, 3\ldots\}$. Consequently, the minimal spacing between harmonics (or spectral lines) is much greater than the cyclic resolution: $\Delta\alpha^{(\min)} = 0.5 \gg \Delta\alpha = 0.0143$; hence respecting the inequality in Eq. (36). In the following the OFACP and OFCMS are applied to the generated signal with 75% overlapping Hanning windows of length $N_h = 128$. This gives a spectral resolution $\Delta f = 150Hz$ fine enough to reveal the spectral content of the distribution. The obtained distributions are displayed in Fig. 3.

Both the distributions are dominated by a significant increase in the spectral frequency band [1.25 kHz, 1.75 kHz] related to the colored stationary noise (and not the AT-CS signal carrier), being continuously distributed along the $\alpha$-axis. Though being weak, the AT-CS patterns are still present in the distribution through parallel spectral lines discretely located at the signal cyclic orders

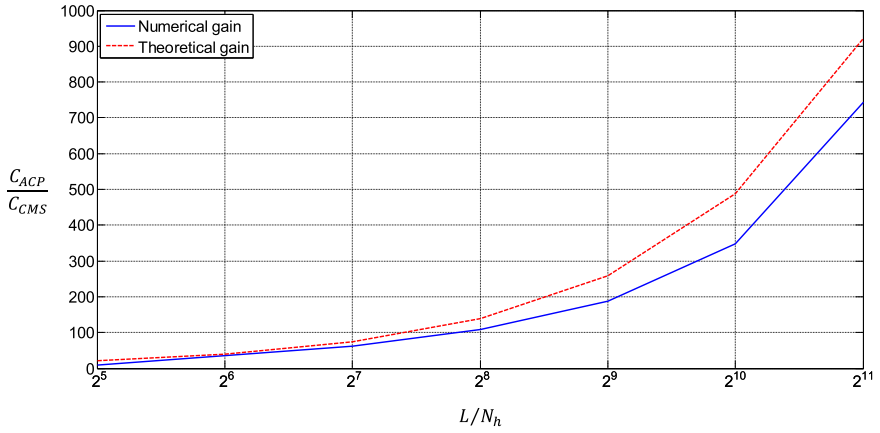


**Fig. 3.** The numerical computational gain averaged over 50 runs (blue continuous line) and theoretical gain (computed through Eq. (35)) of the OFCMS relative to the OFACP for different signal-to-window length ratio.

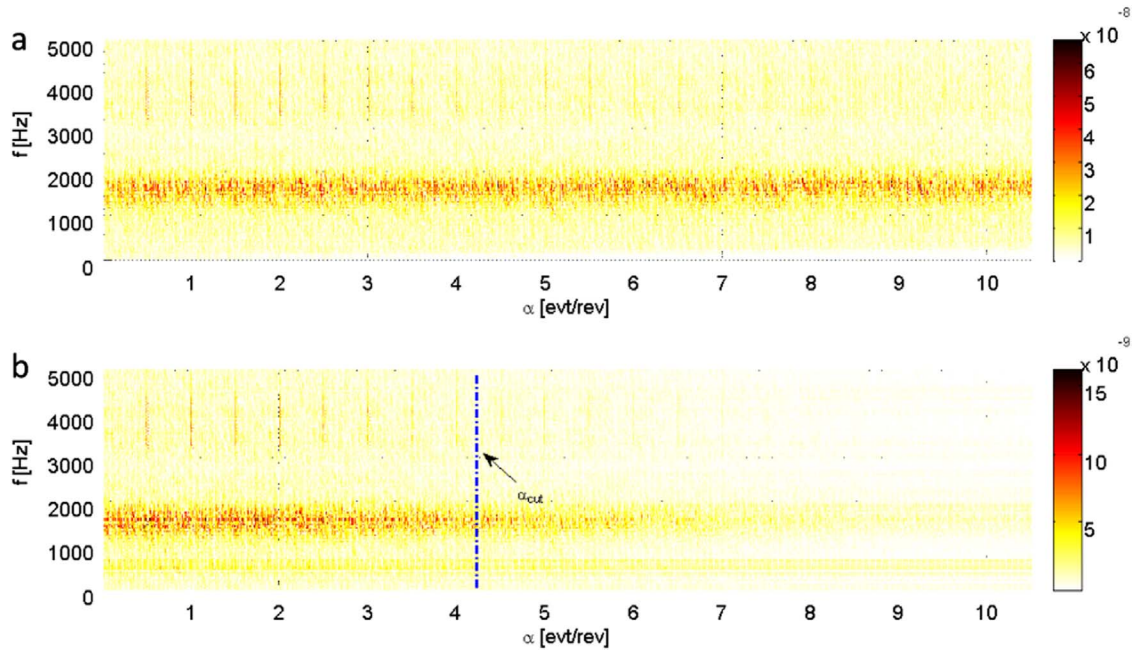


**Fig. 4.** (a) The OFACP and (b) OFCMS applied to an AT-CS signal embedded in a stationary noise. A 75% overlapping Hanning window of length $N_h = 128$ is used for both the estimators. The distributions have the following characteristics: $\Delta\alpha = 0.0143$, $\Delta f = 150Hz$ , a variance reduction $L_t/N_h \approx 312$ and $\alpha_{cut} = 4.25$ (the vertical blue dashed line in (b)).

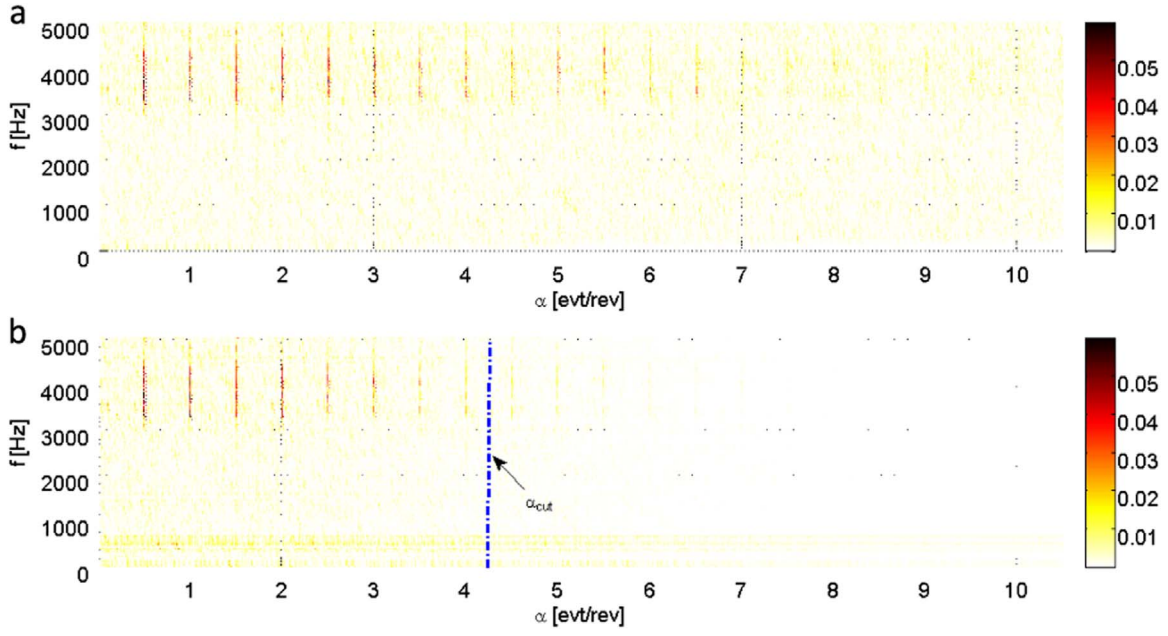


**Fig. 5.** (a) The OFACCoh and (b) the OFCMCoh applied to an AT-CS signal embedded in a stationary noise. A 75% overlapping Hanning window of length $N_h = 128$ is used for both of the estimators. The distributions have the following characteristics: $\Delta\alpha = 0.0143$, $\Delta f = 150Hz$ , a variance reduction $L_t/N_h \approx 312$ and $\alpha_{cut} = 4.25$ (the vertical blue dashed line in (b)).

($\alpha$=0. 5k ; k = 1, 2, …) and whose intensity significantly increases in the carrier frequency band [3 kHz, 4 kHz]. The main difference between the estimators is the gradual decrease in the OFCMS magnitude along the $\alpha$-axis: cyclic information located to the right side of $\alpha_{cut}$ line is almost lost. Evidently, this results from the OFCMS bias which acts as a low-pass filter that filters out all the cyclic orders greater than $\alpha_{cut}$.

As advocated in Ref. [21], a disadvantage of the OFSC is that it highlights the spectral properties of the signal—being of CS or stationary origin—according to their resulting power spectral density. The present case is an example wherein the stationary colored

**Table 1**
Main characteristics of the REB (deep groove MB ER-16K).

| Pitch Diameter [mm] | Rolling element diameter [mm] | Number of rolling elements | Contact angle | Radial load [kg] | Fundamental train order (FTO) | Ball pass order-outer race (BPOO) | Ball pass order-inner race (BPOI) | Ball spinning order (BSO) |
|---|---|---|---|---|---|---|---|---|
| 39.32 | 7.94 | 9 | 0.00 | 5 | 0.399 | 3.592 | 5.41 | 2.376 |

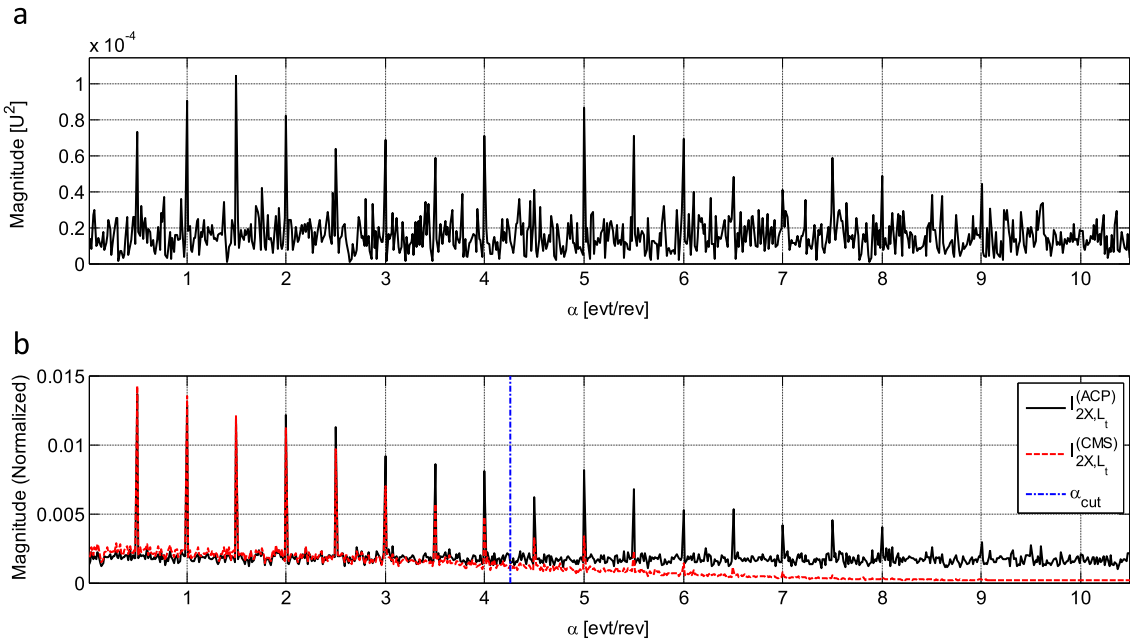


**Fig. 6.** The SES and (b) IES estimators: (i) the ACP-IES (black continuous plot), (ii) the CMS-IES (red dashed plot) and $\boldsymbol{\alpha_{cut}}$ (vertical blue dashed line), applied to the simulated AT-CS signal.

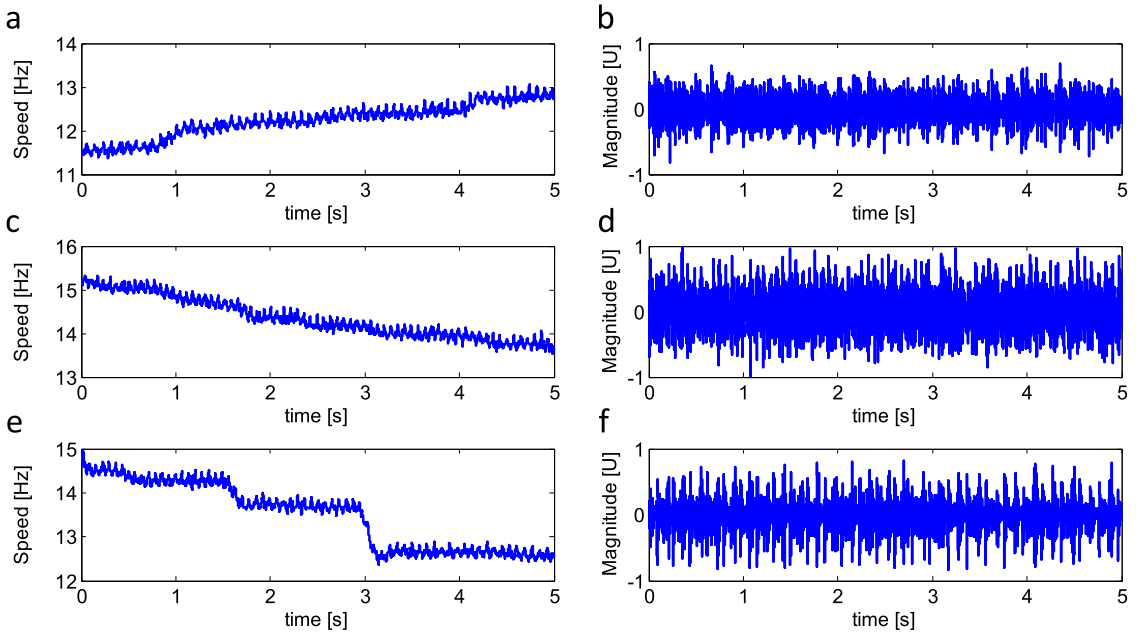


**Fig. 7.** Experiment 1: (a) speed profile, (b) acceleration signal. Experiment 2: (c) speed profile, (d) acceleration signal. Experiment 3: (e) speed profile, (f) acceleration signal.

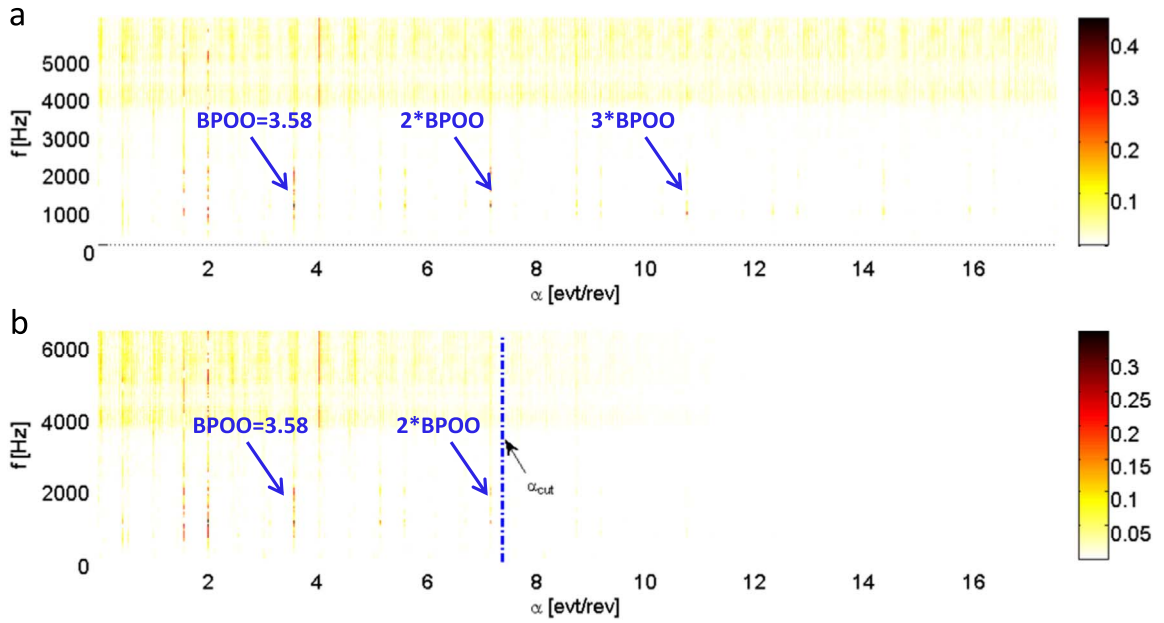


**Fig. 8.** (a) The OFACCoh and (b) the OFCMCoh applied to acceleration signal of experiment 1. A 75% overlapping Hanning window of length $\mathbf{N_h} = 128$ is used for both of the estimators. The distributions have the following characteristics: $\mathbf{\Delta\alpha}$~0. 0079, $\mathbf{\Delta f}$~100**Hz** , a variance reduction $\mathbf{L_t/N_h} \approx 1000$ and $\boldsymbol{\alpha_{cut}} = 7.37$ (the vertical blue dashed line in (b)). Spectral lines which exceed $\boldsymbol{\alpha_{cut}}$ are removed from the OFCMS.

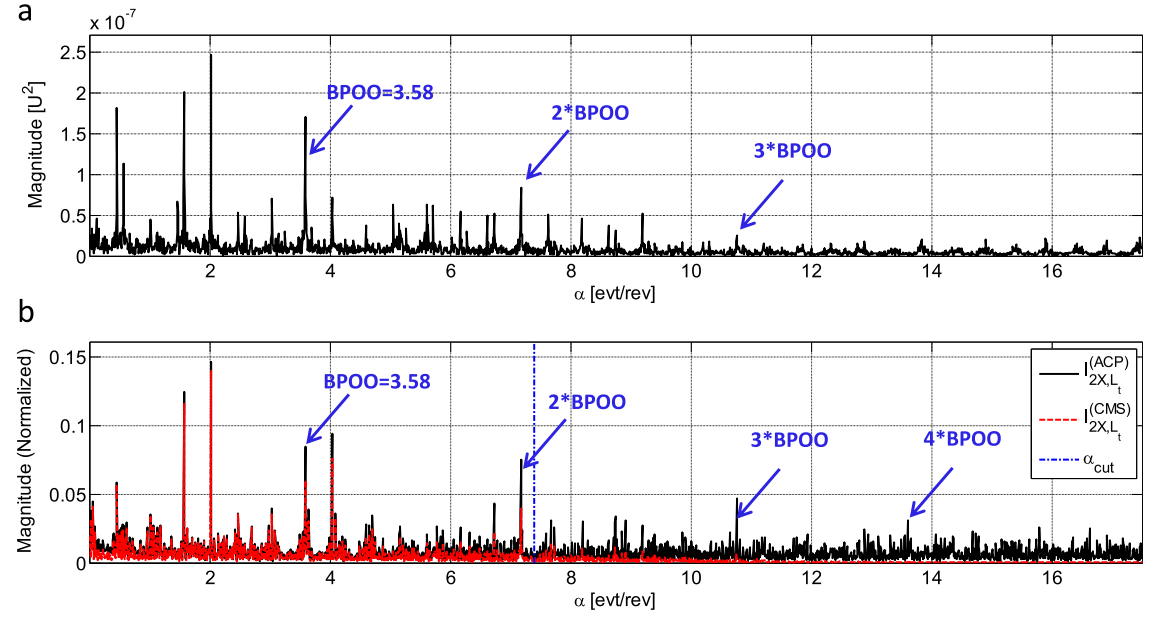


**Fig. 9.** (a) The SES and (b) IES estimators: (i) the ACP-IES (black continuous plot), (ii) the CMS-IES (red dashed plot) and $\boldsymbol{\alpha_{cut}}$ (vertical blue dashed line), applied to the acceleration signal of experiment 1.

noise merely dominates the distributions. In some cases, the stationary noise may completely mask the AT-CS patterns.[13] The OFSCoh presents a straightforward solution to this issue. To see this, the OFACCoh and the OFCMCoh are applied to the simulated signal and the obtained results are displayed in Fig. 4. Interestingly, both the distributions exclusively reveal the patterns related to angle/time cyclostationarity, while those induced by the stationary noise were completely compensated by the implicit whitening operation. Note also that, similarly to the OFCMS, the OFCMCoh is also biased and witnesses a gradual decrease in its magnitude along the $\alpha$-axis.

[13] Interested readers may check this case by reconsidering the previous example with $SNR \geq -15dB$.

Eventually, the IES estimators are computed by averaging the OFACCoh and OFCMCoh over the whole spectral frequency axis, obtaining the ACP-IES and CMS-IES, respectively. The obtained distributions are displayed in Fig. 5 together with the SES for comparison. Obviously, the SES seems much noisier than the IES as the variability of its noise floor is significant, even though most of the harmonics can still be identified. The ACP-IES is the cleanest distribution which can clearly exhibit the full harmonic structure, contrary to the CMS-IES whose efficiency is restricted to $\alpha \ll \alpha_{cut}$. In short, the enhancement seen in the IES is due to (i) the inherent whitening/normalization operation in the OFSCoh which cancels out the effect of non-white stationary noise and (ii) the summation over real-positive value which promotes non-zero component as mentioned in Section 4.2.

### 5.3. Application 1: fault simulator system

The first application investigates the diagnosis of a REB in a simple mechanical chain provided by a machine fault simulator. The dataset used in this paragraph is provided as Supplementary materials in Ref. [46], being accessible from the electronic version of that paper. This section starts by briefly introducing the test rig, before testing the proposed tools on real vibration signals in three cases associated with three distinct REB faults.

*5.3.1. Test rig and experiments.* This subsection describes the principal elements of the test rig and the conducted experiments, while details can be found in the reference source [46]. The test rig under investigation is a Spectra Quest Machine fault simulator system. It consists of a Marathon three phase induction motor of 0.5 HP with speed controller, followed by a simple power transmission chain which includes REBs. A Polytec laser vibrometer is used to measure the vibrations of the system. The sampling frequency of the acquisition system is 50 kHz. Three experiments were conducted in which three REBs with distinct pre-fabricated faults (in outer race, inner race and ball) are used. The principal characteristics of the REB are summarized in Table 1. In each experiment, the speed is manually controlled and the resulting profile is arbitrary varying between 10 and 20 Hz along a 20 s record. In the present paper, only a 10 s portion of the acquisitions (precisely from $t_1$=5$s$ to $t_2$=15$s$) is used to validate the proposed tools. The corresponding speed profiles and acceleration signals are displayed in Fig. 6. These three cases are investigated in the next subsections. Signals are decimated by factor 4 using the built-in 'decimate' MATLAB function so that the corresponding sampling frequency becomes $F_s$=12.5$kHz$ and record length $L_t$=125000.

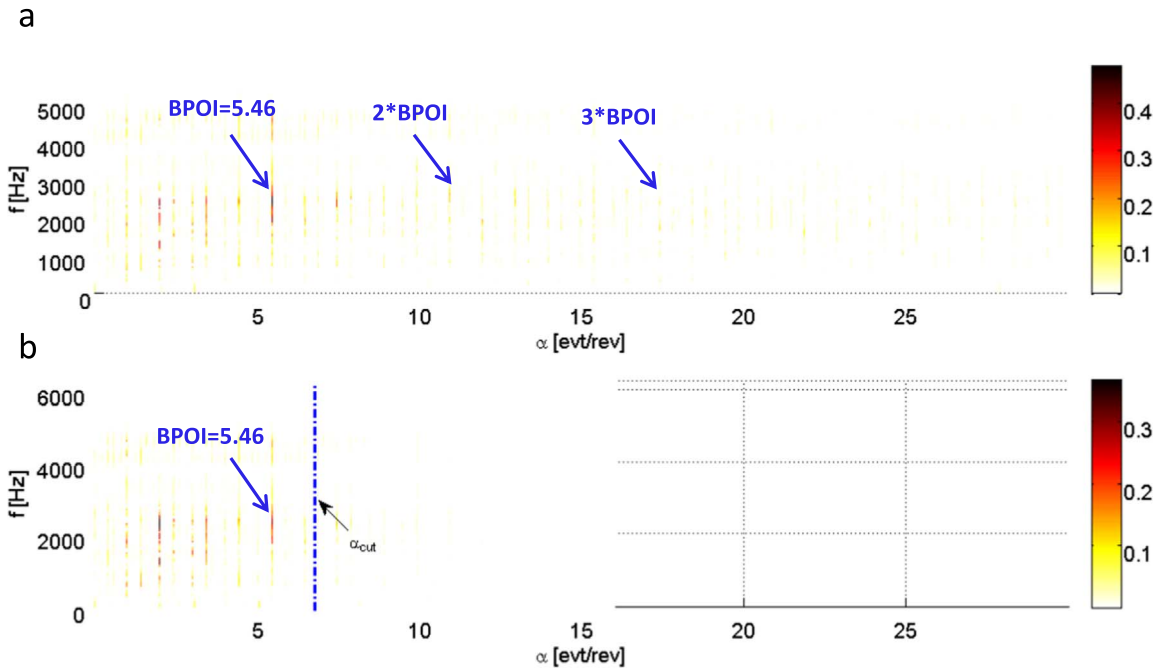


**Fig. 10.** (a) The OFACCoh and (b) the OFCMCoh applied to acceleration signal of experiment 2. A 75% overlapping Hanning window of length $N_h$ = 128 is used for both of the estimators. The distributions have the following characteristics: $\Delta\alpha$~0. 0073, $\Delta f$~100**Hz** , a variance reduction $L_t/N_h \approx 1000$ and $\alpha_{cut}$ = 6.85 (the vertical blue dashed line in (b)).

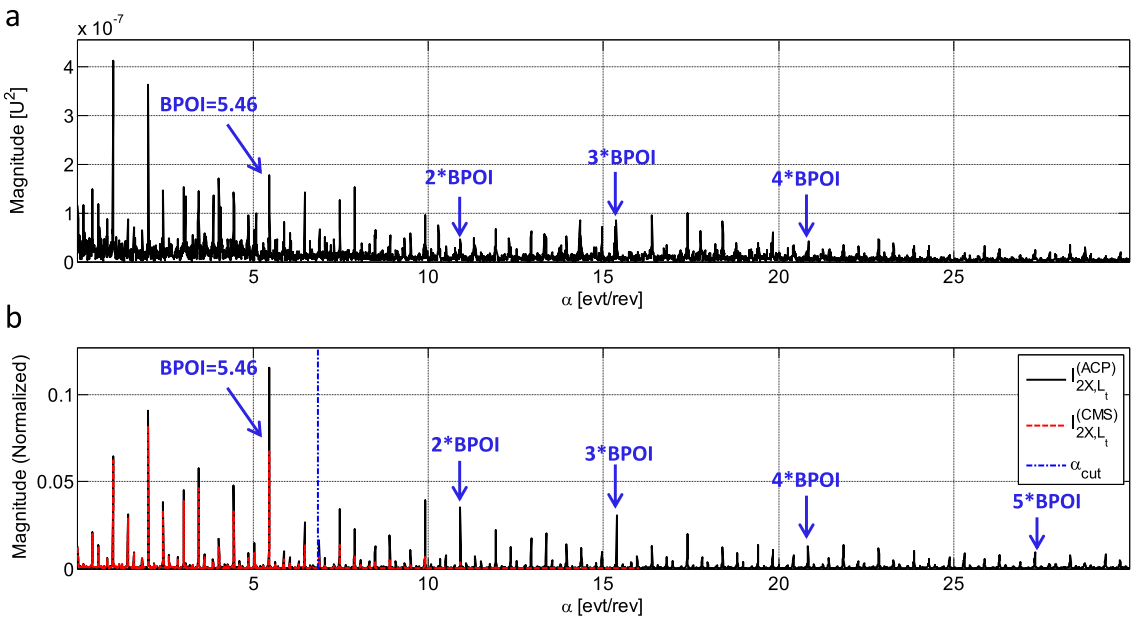


**Fig. 11.** (a) The SES and (b) IES estimators: (i) the ACP-IES (black continuous plot), (ii) the CMS-IES (red dashed plot) and $\boldsymbol{\alpha_{cut}}$ (vertical blue dashed line), applied to the acceleration signal of experiment 2.

*5.3.2. Case 1: outer-race fault.* The OFACCoh and OFCMCoh are applied to the acceleration signal of experiment 1, with 75% overlapping Hanning windows of length $N_h$=128. This gives a spectral resolution $\Delta f$~100$Hz$ which is believed to be fine enough to reveal the spectral content of the distribution. The machine executes almost 127 cycles during the 10 s record, resulting in a cyclic order resolution $\Delta\alpha$~0.0079, fine enough to reveal the cyclic orders of the outer-race fault signature (expected to be spaced apart by $BPOO$ = 3.59). The upper limit of the $\alpha$-axis computed through Eq. (27) is $\alpha_{cut}$=7.37. The obtained distributions are displayed in Fig. 7. The outer-race fault signature is clearly present in the OFACCoh through three spectral lines located at the outer-race fault

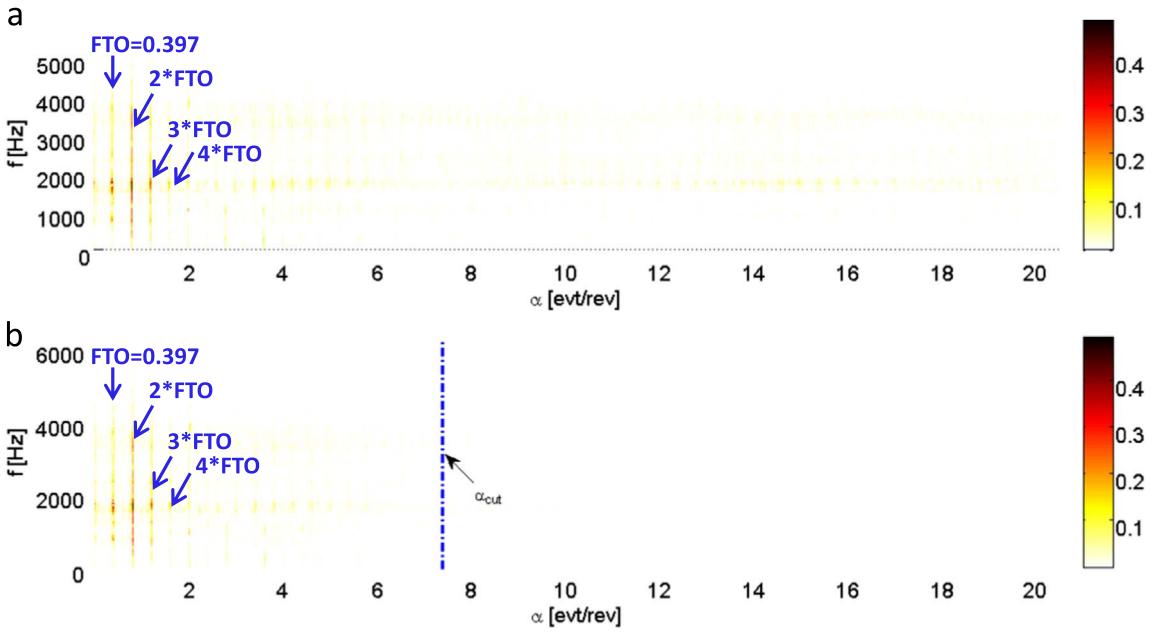


**Fig. 12.** (a) The OFACCoh and (b) the OFCM applied to acceleration signal of experiment 2. A 75% overlapping Hanning window of length $\boldsymbol{N_h}$ = 128 is used for both of the estimators. The distributions have the following characteristics: $\boldsymbol{\Delta\alpha}$~0. 0073, $\boldsymbol{\Delta f}$~100**Hz** , a variance reduction $\boldsymbol{L_t/N_h} \approx$ 1000 and $\boldsymbol{\alpha_{cut}}$ = 6.85 (the vertical blue dashed line in (b)).

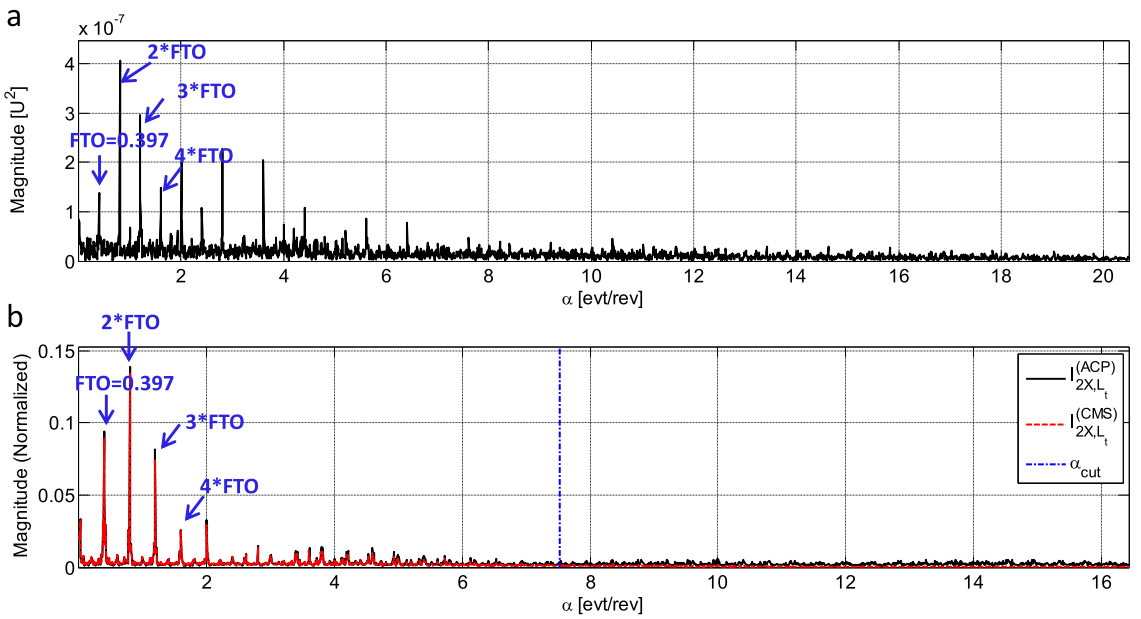


**Fig. 13.** (a) The SES and (b) IES estimators: (i) the ACP-IES (black continuous plot), (ii) the CMS-IES (red dashed plot) and $\boldsymbol{\alpha_{cut}}$ (vertical blue dashed line), applied to the acceleration signal of experiment 3.

order (precisely at 3.58 slightly lower than the theoretical value) and its harmonics. This signature is still present in the OFCMCoh though being less obvious: the magnitude of the second line is significantly attenuated, whereas the third line completely disappears (which is expected as its value exceeds $\alpha_{cut}$).

Later, the ACP-IES and CMS-IES are computed and displayed in Fig. 8 together with the SES for comparison. As expected, the outer-race signature is present in the SES through three visible harmonics. This signature is more clearly present in the ACP-IES due to (i) the decrease of the background level variability and (ii) the enhancement of the fault harmonics (see for instance the considerable enhancement of the third harmonic and the appearance of the fourth). However, only two harmonics related to the fault signature appears in the CMS-IES whereof their magnitudes are weaker than those of the ACP-IES. This is evidently due to the OFCMS bias involved in its computation.

To summarize, the OFACCoh achieves excellent compliance in revealing the fault symptom, unlike the OFCMCoh which returns modest results. The shortcoming of the latter is due to the bias of the OFCMS involved in its computation. Specifically, the bias is influential in this case since the fundamental fault harmonic has the same order of magnitude as $\alpha_{cut}$ ($BPOO \sim 0.48\alpha_{cut}$), so that the related signature is highly distorted. As a consequence, only the ACP-IES is able to provide a significant enhancement over the SES.

*5.3.3. Case 2: Inner-race fault.* In the second experiment, the OFACCoh and OFCMCoh are applied to the acceleration signal with the same estimation parameters, resulting in $\Delta f \sim 100Hz$. The machine executes almost 137 cycles during the 10 s record, resulting in a cyclic order resolution $\Delta\alpha \sim 0.0073$, fine enough to reveal the cyclic orders of the inner-race fault signature (expected to be located at $BPOI = 5.46$ , its harmonics and sidebands spaced by 1). The upper limit of the $\alpha$-axis computed through Eq. (27) is $\alpha_{cut}$=6.85. The obtained distributions are displayed in Fig. 9. The inner-race fault signature is clearly present in the OFACCoh through three spectral lines located at the inner-race fault order (precisely at 5.46 slightly higher than the theoretical value) and its harmonics, as well as some sidebands spaced by 1. For the OFCMCoh, the inner-race fault symptom is only present through one relatively weak spectral line located at the BPOI with a pair of sidebands. The other lines are absent from the distribution as their corresponding cyclic orders exceed $\alpha_{cut}$.

The ACP-IES and CMS-IES are computed and displayed in Fig. 10 together with the SES for comparison. The inner-race

**Table 2**
Characteristic fault orders of the REB supporting L5-shaft referenced to L4-shaft.

| L5-shaft order | FTO | BPOO | BPOI | BSO |
|---|---|---|---|---|
| 1.0163 | 0.438 | 7.8855 | 10.408 | 3.614 |

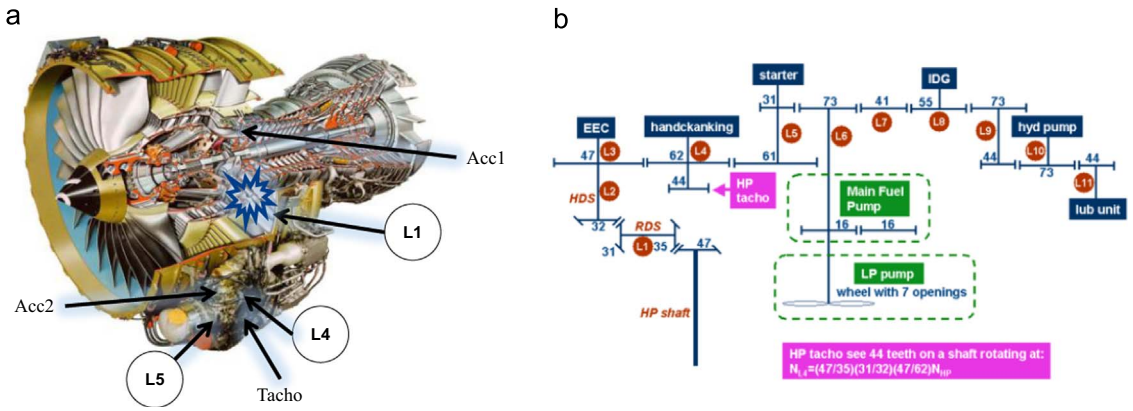


**Fig. 14.** (a) Sensor locations and (b) gearbox kinematics.

signature is present in the SES through four visible harmonics (with some sidebands), being drowned among other shaft related harmonics and relatively high noise floor. For instance, the magnitudes of the shaft order (at one) and its first harmonic exceed that of the BPOI. This signature is so far cleaned and promoted in the ACP-IES due to (i) the decrease of the background noise level variability and (ii) the enhancement of the fault harmonics. In particular, five visible harmonics (with sidebands) can be spotted in the distribution and the BPOI harmonic dominates the distribution (its magnitude exceeds other peaks related to the shaft). However, only one weak harmonic related to the fault signature appears in the CMS-IES. Again, this is due to the OFCMS bias involved in its computation.

To summarize, the OFACCoh achieves excellent compliance in revealing the fault symptom, unlike the OFCMCoh which returns modest results (even worse than in experiment 1). The obvious shortcoming of the latter is due to the fact that the fundamental fault harmonic is close to $\alpha_{cut}$ ($BPOI \sim 0.8\alpha_{cut}$), so that the related cyclic components are either significantly attenuated or rejected because of the OFCMS bias. In this case also, only the ACP-IES is able to provide a significant enhancement over the SES.

*5.3.4. Case 3: Rolling element fault.* In the third experiment, the OFACCoh and OFCMCoh are applied to the acceleration signal with the same estimation parameters, resulting in $\Delta f \sim 100Hz$. The machine executes almost 124 cycles during the 10 s record, resulting in a cyclic order resolution $\Delta\alpha \sim 0.0081$, fine enough to reveal the cyclic orders of the rolling element fault signature (expected to be located at $FTO = 0.339$). The upper limit of the $\alpha$-axis computed through Eq. (27) is $\alpha_{cut}=7.53$. The obtained distributions are displayed in Fig. 11. The corresponding fault signature is identically present in both estimators through three spectral lines located at the inner-race fault order (precisely at 0.397 slightly lower than the theoretical value) and its harmonics.

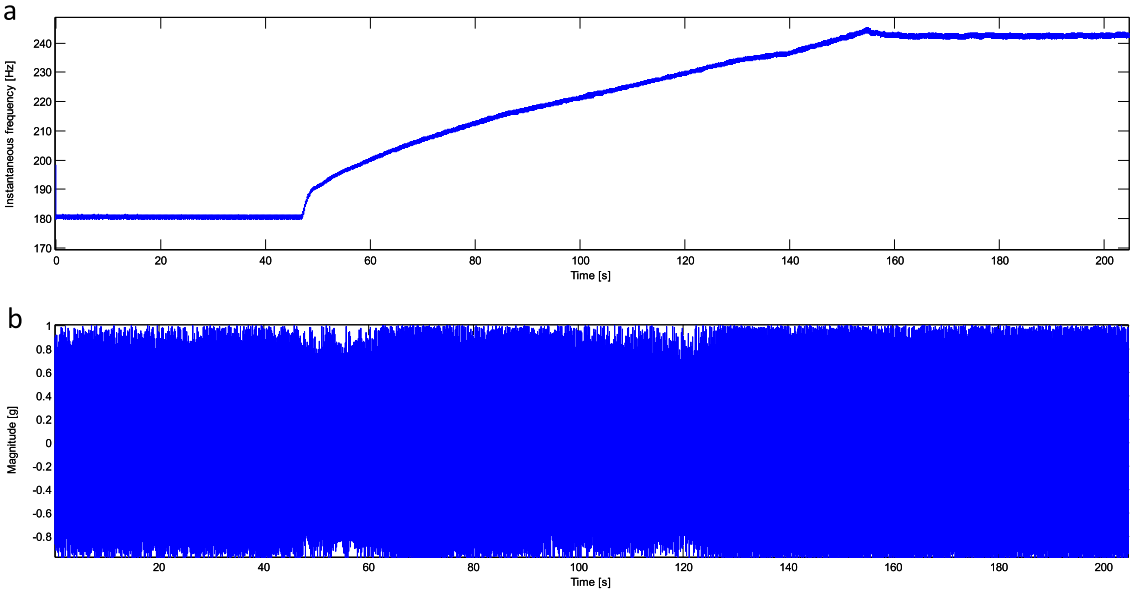


**Fig. 15.** (a) L4-shaft speed profile and (b) signal Acc2.

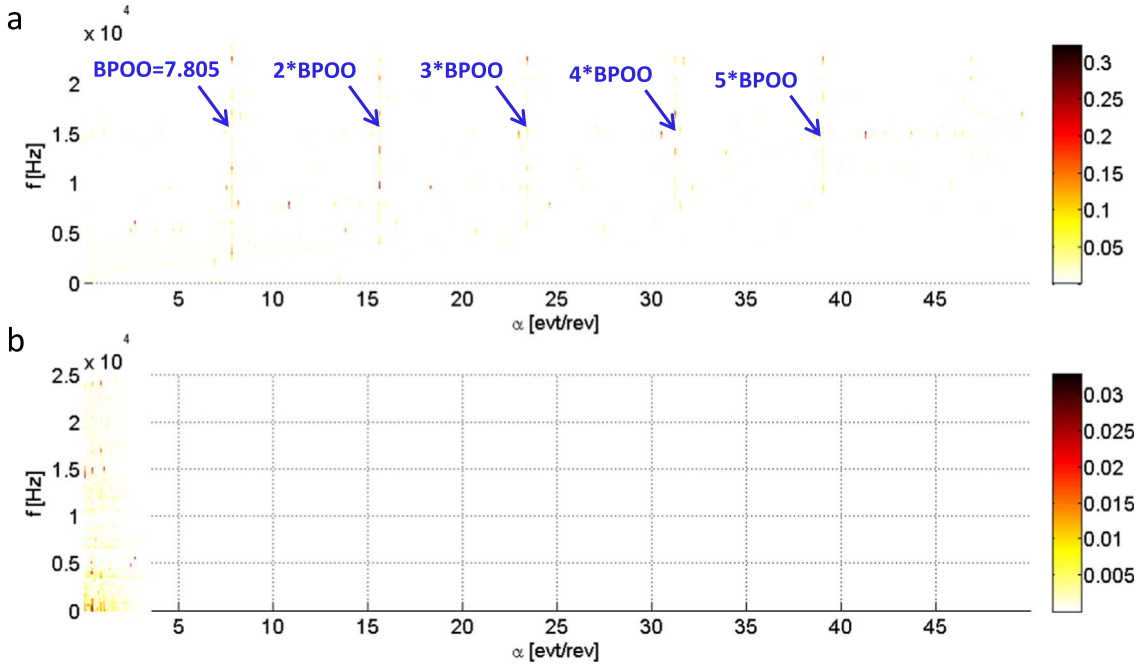


**Fig. 16.** (a) The OFACCoh and (b) the OFCMCoh applied to signal Acc2. A 75% overlapping Hanning window of length $\mathbf{N_h} = 128$ is used for both of the estimators. The distributions have the following characteristics: $\mathbf{\Delta\alpha}$~0.0022, $\mathbf{\Delta f}$~100**Hz** , a variance reduction $\mathbf{L_t/N_h} \approx 780$ and $\mathbf{\alpha_{cut}} = 1.61$.

The IES estimators are then computed by averaging the OFACCoh and OFCMCoh over the whole $f$-axis and the obtained distributions are displayed in Fig. 12 together with the SES. The fault signature is present in the SES through four visible harmonics. This signature is cleaned and promoted in the IES for both estimators due to (i) the decrease in the background noise and (ii) the attenuation/suppression of other harmonic not related to the fault (these harmonics are probably of deterministic origin). Unlike the

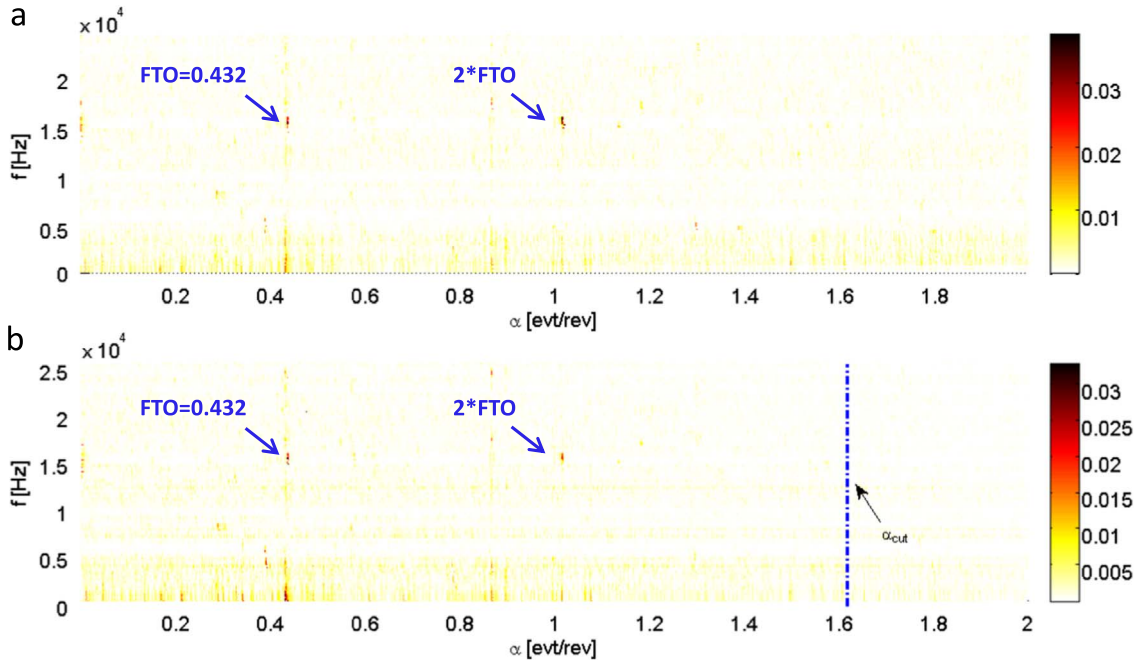


**Fig. 17.** Close-ups of the plots in Fig. 16 between $\mathbf{\alpha}_1 = 0$ to $\mathbf{\alpha}_1 = 2$.

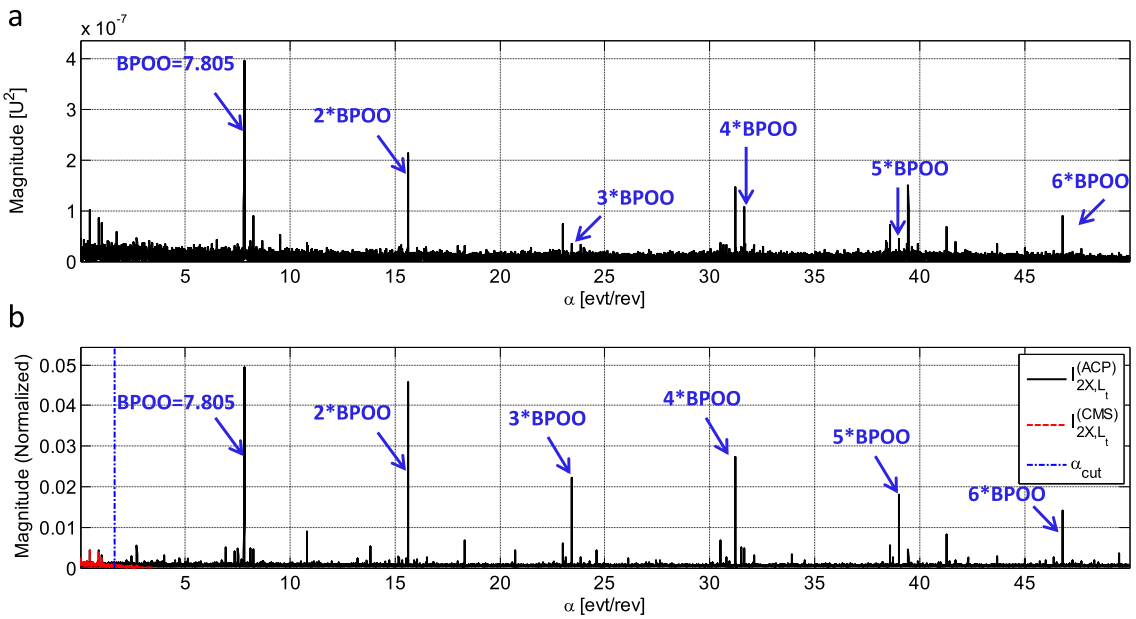


**Fig. 18.** (a) The SES and (b) IES estimators: (i) the ACP-IES (black continuous plot), (ii) the CMS-IES (red dashed plot) and $\boldsymbol{\alpha}_{\mathbf{cut}}$ (vertical blue dashed line), applied to signal Acc2.

previous experiments, the fault signature is identically present in both estimators.

To summarize, the OFACCoh and OFCMCoh both achieve excellent compliance in revealing the fault symptom. The reason behind this is that the fault signature is located in a low cyclic order band, being far away from $\alpha_{cut}$ ($FTO \sim 0.04\alpha_{cut}$): the OFCMS bias is flat and the fault harmonics is thus not distorted. In this case, the use of CMS-based tools is more advantageous since they enjoy lower computational cost.

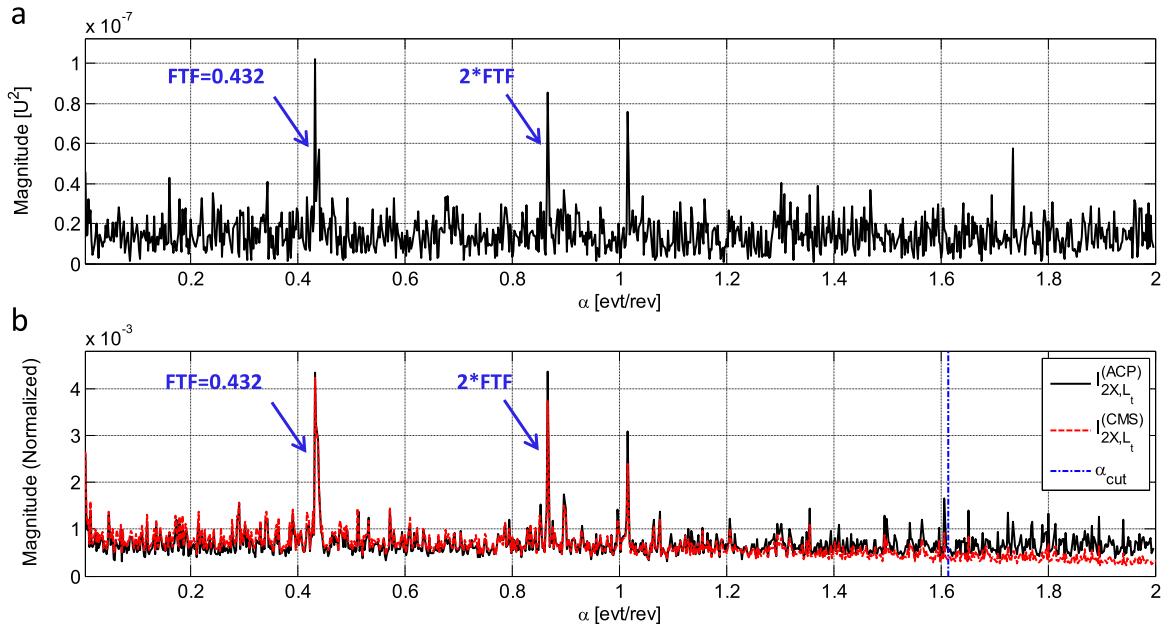


**Fig. 19.** Close-ups of the plots in Fig. 18 between $\boldsymbol{\alpha}_1 = 0$ to $\boldsymbol{\alpha}_1 = 2$.

### 5.4. Application 2: a civil aircraft engine

The second application investigates the diagnosis of a REB in a complex gearbox system of a civil aircraft engine. This issue was displayed in the second exercice of "Safran contest" which has appeared in the conference "Surveillance 8" [49]. The dataset are provided by the company "Snecma" of the group "Safran". The system under investigation is shown in Fig. 13. This part particularly investigates the fault detection of the REB located on shaft L5 through the acquired acceleration signal Acc2. A measure of the angle position (i.e. the speed profile) can be obtained through the tachometer "Tacho". The characteristic fault orders of the REB referenced to the shaft L4 are displayed in Table 2. The sampling frequency equals 50 kHz. The acceleration signal acquired by Acc2 and the L4-shaft speed profile are displayed in Fig. 14. In the analysis, only a 2 s portion of the acquisitions chosen in the runup regime (precisely from $t_1$=125$s$ to$t_2$=127$s$) is used to validate the proposed tools. The record length is then $L_t$=100000.

In a first stage, the OFACCoh and OFCMCoh are applied to signal Acc2, with 75% overlapping Hanning windows of length $N_h$=128. This gives a spectral resolution $\Delta f$~400$Hz$ which is believed to be fine enough to reveal the spectral content of the distribution. The machine executes almost 465 cycles during the 2 s record, resulting in a cyclic order resolution $\Delta\alpha$~0.0022, fine enough to reveal any set of cyclic orders generated by any kind of defect (see Table 2). The upper limit of the $\alpha$-axis computed through Eq. (27) is $\alpha_{cut}$=1.61. The obtained distributions are displayed in Fig. 15 in a wide cyclic order range ($\alpha\in$]0,50]). The outer-race fault signature is strongly present in the OFACCoh through five spectral lines located at the outer-race fault order (precisely at 7.805 slightly lower than the theoretical value) and its harmonics. This signature is totally absent from the OFCMCoh as the value of the BPOO highly exceeds that of $\alpha_{cut}$. Fig. 16 shows the close-ups of the plots in Fig. 15 in the low cyclic order range ($\alpha\in$]0,2]). Interestingly, both distributions reveal two spectral lines at the FTO (precisely at 0.432 slightly lower than the theoretical value) and its harmonic around the spectral frequency 15 kHz. Since the cyclic content of these lines is safely smaller than $\alpha_{cut}$, the OFCMCoh was able this time to reveal the signature. This signature, however, is much weaker than that generated by the outer race.

Next, the ACP-IES and CMS-IES are computed and displayed in Fig. 17 ($\alpha\in$]0,50]) and Fig. 18 ($\alpha\in$]0,2]) . As expected, the outer-race signature is present in the SES through six visible peaks. This signature is more clearly present in the ACP-IES due to (i) the decrease in the noise floor variability and (ii) the enhancement of the fault harmonics and (iii) the attenuation of non-related harmonics. However, the CMS-IES completely fails to reveal any harmonic. For the cage fault signature, two harmonics related to the FTO and its harmonic are detected by the SES and both estimators of the IES, with a slight enhancement in the latter (both IES estimators) over the former (the SES) (Fig. 19).

To summarize, the AT-CS analysis has revealed the presence of an outer race fault and potentially another fault in the cage or the rolling elements. The former was exclusively detected by the ACP-based estimators, whereas the latter was revealed by both estimators. Again, the CMS-based estimators are only valid when the cyclic order of the fault signature is lower than $\alpha_{cut}$.

## 6. Conclusion

The theory of angle/time cyclostationary (AT-CS) signals proves itself as an optimal framework to analyze machine signals in variable speed conditions. Being built upon rigorous theoretical foundations, it offers a wide variety of robust tools able to reveal weak cyclic signature embedded in strong environmental noise. Some tools have been previously addressed, while others are still waiting for their formalization within this scope. The present paper has contributed in this direction by enriching this framework with new tools excerpted from cyclostationarity.

In particular, the practical issues of estimating the "order-frequency spectral correlation" (OFSC) are investigated by proposing a *fast* estimator based on the "cyclic modulation spectrum". The newly introduced estimator, namely the "order-frequency cyclic modulation spectrum" (OFCMS), has been compared with the previously proposed "order-frequency averaged cyclic periodogram" (OFACP) in terms of resolution, statistical performance and computational cost. In addition, the (squared-magnitude) "order-frequency spectral coherence" (OFSCoh)—the normalized/whitened version of the OFSC— has been equally investigated. In this context, its optimality in revealing AT-CS components independently of the signal power spectrum has been theoretically demonstrated. Also, an enhanced envelope spectrum, namely the "improved envelope spectrum", has been derived from the OFSCoh by integrating over the spectral frequency variable. Further, the estimation of the OFSCoh and IES has been proposed through the OFACP and OFCMS, and eventually validated on simulated and real vibration signals in various cases.

Overall, one may exploit the (very) low computational cost of the OFCMS—as well as its derivated tools— to reveal nearly the same information as contained in the OFACP with similar statistical performance, but for particular configurations. Specifically, the component of interest should rotate at moderate speed to ensure a tradeoff between a reasonable spectral frequency resolution and an upper bound (cutoff) cyclic order sufficiently larger than the expected cyclic signature. Otherwise, the use of the OFACP-based tools is mandatory for a better evaluation of the cyclic signatures in machine signals.

## Acknowledgements

This work was performed within the framework of the LabExCeLyA ("Centre Lyonnais d'Acoustique", ANR-10-LABX-60).

## Appendix A. Proof of Eq. (4)

The instantaneous autocorrelation function of an AT-CS signal reads:

$$R_{2X}(t,\ \tau) = \sum_k \sum_{k'} \mathbb{E}\{c_X^k(t) c_X^{k'}(t-\tau)^*\} e^{j(k\theta(t)-k'\theta(t-\tau))}. \tag{A1}$$

Performing a Taylor expansion of $\theta(t)$ around $t-\tau$, one obtains

$$\theta(t-\tau) = \theta(t) - \sum_{n=0}^{+\infty} \frac{\omega^{(n)}(t-\tau)}{(n+1)!}\tau^n, \tag{A2}$$

where $\omega^{(n)}(t) = \partial^n \omega(t)/\partial t^n$ denotes the $n^{th}$ derivative of the angular speed $\omega(t)$. Assuming a slow evolution of the speed and of its derivatives as compared to the time-lag $\tau$ (i.e. $\omega^{(n)}(t) = \omega^{(n)}(t-\tau)$ for all $\tau$, $n$) and substituting Eq. (A2) in Eq. (A1), one can express the instantaneous autocorrelation functions as

$$R_{2X}(t,\ \tau) = \sum_k \sum_{k'} \{c_{2X}^{k,k'}(\tau) g^{k'}(\tau, \omega(t),\ \omega^{(1)}(t),\ \omega^{(2)}(t)\ldots)\} e^{j(k-k')\theta(t)}, \tag{A3}$$

where $c_{2X}^{k,k'}(\tau) = \mathbb{E}\{c_X^k(t) c_X^{k'}(t-\tau)^*\}$ denotes the correlation between the stationary coefficients $c_X^k(t)$ and $c_X^{k'}(t)$ and

$$g^{k'}(\tau, \omega, \omega^{(1)},\ \omega^{(2)}\ldots) = \prod_{n=0}^{+\infty} e^{jk' \frac{\omega^{(n)}(t)}{(n+1)!}\tau^{n+1}}. \tag{A4}$$

Applying the variable change $t = t(\theta)$ and manipulating the summation bounds, one obtains the AT-CF

$$\mathfrak{R}_{2X}(\theta,\ \tau) = \sum_k \mathfrak{R}_{2X}^k(\tau,\ \tilde{\omega}(\theta),\ \tilde{\omega}^{(1)}(\theta),\ldots) e^{jk\theta} \tag{A5}$$

where

$$\mathfrak{R}_{2X}^k(\tau,\ \tilde{\omega},\ \tilde{\omega}^{(1)},\ldots) = \sum_{k'} \{c_{2X}^{k+k',k'}(\tau) g^{k'}(\tau,\ \tilde{\omega},\ \tilde{\omega}^{(1)},\ldots)\} \tag{A6}$$

and $\tilde{\omega}^{(n)}(\theta) = \omega^{(n)}(t(\theta))$ stands for the $n^{th}$ speed derivative profile in the angular domain. It is clear that the cyclic autocorrelation function $\mathfrak{R}_{2X}^k$ depends on the angle through the functions $g^{k'}(\tau, \tilde{\omega}(\theta),\ \tilde{\omega}^{(1)}(\theta)\ldots)$ which, in turn, have an explicit dependence on the speed and its derivatives. The functions $g^{k'}$ only distort the phase as its moduli equals one. Also, the smoother the speed is, the less the induced phase distortions are. Therefore, these functions have a minor effect on the global statistical analysis. By considering the speed profile and its derivatives as random variables, one obtains on the average

$$\mathbb{E}_{\tilde{\omega},\tilde{\omega}^{(1)}\ldots}\{\mathfrak{R}_{2X}^k(\tau,\ \tilde{\omega},\ \tilde{\omega}^{(1)},\ldots)\} = \sum_{k'} \{c_{2X}^{k+k',k'}(\tau) G^{k'}(\tau)\} \tag{A7}$$

where

$$G^{k'}(\tau) = \lim_{n\to+\infty} \int_{\tilde{\omega}} \ldots \int_{\tilde{\omega}^{(n)}} g^{k'}(\tau,\ \tilde{\omega},\ \tilde{\omega}^{(1)},\ \ldots \tilde{\omega}^{(n)}) f(\tilde{\omega},\ \tilde{\omega}^{(1)},\ \ldots \tilde{\omega}^{(n)}) d\tilde{\omega}^{(1)} d\tilde{\omega}^{(2)} \ldots d\tilde{\omega}^{(n)} \tag{A8}$$

and $f(\tilde{\omega},\ \tilde{\omega}^{(1)},\ldots\tilde{\omega}^{(n)})$ denotes the joint probability density function of $\tilde{\omega},\ \tilde{\omega}^{(1)},\ldots\tilde{\omega}^{(n)}$.

Taking Eq. (A7) into account, the rest of the proof follows with

$$\mathfrak{R}_{2X}^k(\tau) = \sum_{k'} \{c_{2X}^{k+k',k'}(\tau) G^{k'}(\tau)\}. \tag{A9}$$

## Appendix B. Matlab routine of the OFCMS

```
function [Px,F,A] = OFCMS(x,theta,wind,Noverlap,nfft,Fs)
%%% Function description
%%% This function computes the order-frequency cyclic modulation spectrum
%%% with unit [U^2/Hz] based on the overlap-add (OLA)algorithm.
%%% Inputs:
%%%     x: time signal
%%%     theta: angular position profile in randians
%%%     wind: -if wind is a vector, it is considered as the window
%%%           -if wind is an integer, it corresponds to the length of a
%%%            a Hamming window used by default.
%%%     noverlap: the number of samples that each segment overlaps.
%%%     nfft: the FFT length
%%%     Fs: the sampling frequency
%%% Outputs:
%%%     Px: the order-frequency cyclic modulation spectrum
%%%     F: the spectral frequency axis (only positive frequencies)
%%%     A: the cyclic order axis (only positive orders)
% ----------------------
% D. Abboud & J. Antoni: 02/2016
% ----------------------


 % Step 1: Time-frequency spectrogram

[STFT,F,T,TF_IPS] = spectrogram(x,wind,Noverlap,nfft,Fs);
TF_IPS=TF_IPS/2/length(x); % Normalization

% Step 2: Time to angle COT --> angle-frequency spectrogram

Delta_T=T(2)-T(1); %decimated temporal sampling period of the spectrogram
fr_min=min(Fs*diff(theta)/2/pi); % compute the minimal shaft frequency
SmpPerRev=1+fix(1/Delta_T/fr_min); % use the lowest allowable number of
samples per rev. to avoid aliasing
thetaxis_var= interp1((0:length(x)-1)/Fs,theta,T,'spline'); %the angular
position of the spectrogram time axis
thetaxis_cte = thetaxis_var(1):2*pi/SmpPerRev:thetaxis_var(end);  % Constant-
angle increment axis
t2 = interp1(thetaxis_var,1:length(thetaxis_var),thetaxis_cte,'spline'); %
find the time instants (in bins) related to constant angular increments
AF_IPS = interp1(1:length(TF_IPS'),TF_IPS',t2,'spline'); %angle-frequency
spectrogram

% Step 3: angle-to-order Fourier transform--> OFCMS

Px=fft(AF_IPS)/length(AF_IPS);
do=SmpPerRev/length(AF_IPS); %the order increment
A=0:do:do*length(AF_IPS)/2; %the order axis
Px=Px(1:length(A),:); %take the one-sided transform
```

.

## References


[1] F. Bonnardot, R.B. Randall, F. Guillet, Extraction of second-order cyclostationary sources—application to vibration analysis, Mech. Syst. Signal Process. 19 (6) (2005) 1230–1244.
[2] R. Boustany, J. Antoni, A subspace method for the blind extraction of a cyclostationary source: application to rolling element bearing diagnostics, Mech. Syst. Signal Process. 19 (6) (2005) 1245–1259.
[3] R. Boustany, J. Antoni, Blind extraction of a cyclostationary signal using reduced-rank cyclic regression—a unifying approach, Mech. Syst. Signal Process. 22 (3) (2008) 520–541.
[4] M.S. Bartlett, Smoothing periodograms from time-series with continuous spectra, Nature 161 (1948) 686–687.
[5] D.J. Thomson, Spectrum estimation and harmonic analysis, Proc. IEEE 70 (1982) 1055–1096.
[6] D. Hanson, R.B. Randall, J. Antoni, D.J. Thompson, T.P. Waters, R.A.J. Ford, Cyclostationarity and the cepstrum for operational modal analysis of MIMO systems—part I: modal parameter identification, Mech. Syst. Signal Process. 21 (6) (2007) 2441–2458.
[7] R. Boustany, J. Antoni, Cyclic spectral analysis from the averaged cyclic periodogram, in: Proceedings of the 16th IFAC World Congress, Prague, Czech Republic, July 4–8, 2005.
[8] W.A. Gardner, The spectral correlation theory of cyclostationary time-series, Signal Process. 8 (1986).
[9] W. Gardner, Measurement of spectral correlation, IEEE Trans. Acoust. Speech Signal Process. 34 (5) (1986) 1111–1123.
[10] R. Roberts, W. Brown, H. Loomis, Computationally efficient algorithms for cyclic spectral analysis, IEEE Signal Process. Mag. (1991) 38–49.
[11] W. Gardner, Exploitation of spectral redundancy in cyclostationary signals, IEEE Signal Process. Mag. 8 (2) (1991) 14–36.
[12] A. Raad, J. Antoni, M. Sidahmad, Indicators of cyclostationarity: theory and application to gear fault monitoring, Mech. Syst. Signal Process. 22 (3) (2008) 574–587.
[13] W.A. Gardner, A. Napolitano, L. Paura, Cyclostationarity: half a century of research, Signal Process. 86 (4) (2006) 639–697.
[14] P. Borghesani, P. Pennacchi, R. Ricci, S. Chatterton, Testing second order cyclostationarity in the squared envelope spectrum of non-white vibration signals, Mech. Syst. Signal Process. 40 (1) (2013) 38–55.
[16] H. Hermansky, Modulation spectrum in speech processing, in: A., Procházka, J. Uhlíř, P.W.J. Rayner, N.G. Kingsbury (Eds.), Signal Analysis and Prediction, Birkhäuser Boston, Boston, 1998, pp. 395–406 (Print).
[17] L. Atlas, S. Greenberg, H. Hermansky, The Modulation Spectrum and its Application to Speech Science and Technology, Interspeech 2007, Antwerp, Belgium, 2007.
[18] R.B. Randall, J. Antoni, S. Chobsaard, The relationship between spectral correlation and envelope analysis for cyclostationary machine signals, application to ball bearing diagnostics, Mech. Syst. Syst. Process. 15 (5) (2001) 945–962.
[19] J. Antoni, D. Abboud, S. Baudin, Time-angle periodically correlated process, Cyclostationarity: theory and methods, Lecture Notes in Mechanical Engineering, Springer, 2014.
[20] J. Antoni, N. Ducleaux, G. NGhiem, S. Wang, Separation of combustion noise in IC engines under cyclo-non-stationary regime, Mech. Syst. Signal Process. 38 (1) (2009) 223–236.
[21] D. Abboud, S. Baudin, J. Antoni, D. Remond, M. Eltabach, O. sauvage, The spectral correlation analysis of cyclo-non-stationary signals, Mech. Syst. Signal Process. 75 (2016) 280–300.
[22] D. Abboud, J. Antoni, M. Eltabach, S. Sieg-Zieba, Angle/time cyclostationarity for the analysis of rolling element bearing vibrations, Measurements 75 (2015) 29–39.
[23] J. Antoni, Cyclic spectral analysis in practice, Mech. Syst. Signal Process. 21 (2007) 597–630.
[24] J. Antoni, Cyclic spectral analysis of rolling-element bearing signals: facts and fictions, J. Sound Vib. 304 (2007) 497–529.
[25] Malcolm J. Crocker, Handbook of Acoustics, John Wiley & Sons, Hoboken, New Jersey, États-Unis, 1998.
[26] K.R. Fyfe, E.D.S. Munck, Analysis of computed order tracking, Mech. Syst. Signal Process. 11 (2) (1997) 187–205.
[27] S. Baudin, D. Rémond, J. Antoni, O. Sauvage, Non-intrusive rattle noise detection in non-stationary conditions by an angle/time cyclostationary approach, J. Sound Vib. 366 (2016) 501–513.
[28] F. Bonnardot, M. ElBadaoui, R.B. Randall, J. Daniere, F. Guillet, Use of the acceleration signal of a gearbox in order to perform order tracking (with limited speed fluctuation), Mech. Syst. Signal Process. 19 (2005) 766–785.
[29] Alan V. Oppenheim, Ronald W. Schafer, Digital Signal Processing, Prentice-Hall, Englewood Cliffs, N.J., 1975 (ISBN 0-13-214635-5).
[31] T.G. Stockham, High Speed Convolution and Correlation, in: Proceedings of the Spring Joint Computer Conference, AFIPS January 1966. doi: ⟨http://doi.org/10.1145/1464182.1464209⟩.
[32] P.D. Welch, The use of fast fourier transform for the estimation of power spectra: a method based on time averaging over short, modified periodograms, IEEE Trans. Audio Electro., AU- 15 (1967) 70–73.
[33] Z. Feng, M. Liang, F. Chu, Recent advances in time–frequency analysis methods for machinery fault diagnosis: a review with application examples, Mech. Syst. Signal Process. 38 (2013) 165–205.
[34] J.G. Proakis, D.G. Manolakis, Digital Signal Processing – Principles, Algorithms, and Applications, 3rd ed., Prentice-Hall, Englewood Cliffs, NJ, 1996.
[35] J.O. Smith, Spectral Audio Signal ProcessingW3K Publishing (2011), 2011 (ISBN 978-0-9745607-3-).
[36] J. Urbanek, T. Barszcz, J. Antoni, Time–frequency approach to extraction of selected second-order cyclostationary vibration components for varying operational conditions, Measurement 46 (2013) 1454–1463.
[37] J. Antoni, D. Hanson, Detection of surface ships from interception of cyclostationary signature with the cyclic modulation coherence, IEEE J. Ocean. Eng. 37 (3) (2012).
[38] R.B. Randall, J. Antoni, Rolling element bearing diagnostics—a tutorial, Mech. Syst. Sig. Process., vol. 25(2), pp. 485–520.
[39] R.B. Randall, Vibration-Based Condition Monitoring: Industrial, Automotive and Aerospace Applications, John Wiley and Sons, West Sussex, 2011.
[40] F.J. Harris, On the use of windows for harmonic analysis with the discrete Fourier transform, Proc. IEEE 66 (1978) 51–83.
[41] J.O. Smith, X. Serra, PARSHL: an analysis/synthesis program for non-harmonic sounds based on a sinusoidal representation, in: Proceedings of the International Computer Music Conference (ICMC-87, Tokyo),Computer Music Association, 1987.
[42] M.W. Trethewey, Window and overlap processing effects on power estimates from spectra, Mech. Syst. and Signal Process. 14 (2) (2000) 267–278.
[43] G. Heinzel, A. Rüdiger, R. Schilling, Spectrum and spectral density estimation by the Discrete Fourier transform (DFT), including a comprehensive list of window functions and some new at-top windows, Scientific Report, 2002. ⟨http://hdl.handle.net/11858/00-001M-0000-0013-557A-5⟩.
[44] P. Borghesani, P. Pennacchi, S. Chatterton, R. Ricci, The velocity synchronous discrete Fourier transform for order tracking in the field of rotating machinery 44 (1–2) (2014) 118–133.
[45] H. André, Z. Daher, J. Antoni, D. Rémond, Comparison between angular sampling and angular re-sampling methods applied to the vibration monitoring of a gear meshing in non-stationary conditions, Proc. ISMA 2010 Incl. USD (2010).
[46] C. Mishra, et al., Rolling element bearing defect diagnosis under variable speed operation through angle synchronous averaging of wavelet de-noised estimate, Mech. Syst. Signal Process (2015).
[47] P. Borghesani, The envelope-based cyclic periodogram, Mech. Syst. Signal Process. 58-59 (2015) 245–270.
[48] J. Antoni, Ge Xin, N. Hamzaoui, Fast computation of the spectral correlation, Mech. Syst. Signal Process. (2016) (in preparation).
[49] SAFRAN Contest, Conference Surveillance, Roanne, France, vol. 8, October 20–21, 2015.
[50] R. Zimroz, W. Bartelmus, Tomasz Barszcz, Jacek Urbanek, Diagnostics of bearings in presence of strong operating conditions non-stationarity—a procedure of load-dependent features processing with application to wind turbine bearings, Mech. Syst. Signal Process. 46 (1) (2014) 16–27.
[51] W. Bartelmus, F. Chaari, R. Zimroz, Mohamed Haddar, Modelling of gearbox dynamics under time-varying nonstationary load for distributed fault detection and diagnosis, Eur. J. Mech. - A/Solids 29 (4) (2010) 637–646.

[52] D. Abboud, J. Antoni, S. Sieg-Zieba, M. Eltabach, Envelope analysis of rotating machine vibrations in variable speed conditions: a comprehensive treatment, Mech. Syst. Signal Process. 84 (2017) 200–226.
[53] Jacek Urbanek, Tomasz Barszcz, Adam Jablonski, Application of Angular–Temporal Spectrum to Exploratory Analysis of Generalized Angular–Temporal Deterministic Signals.
[54] Jacek Urbanek, Tomasz Barszcz, Marcin Strączkiewicz, Adam Jablonski, Jacek Urbanek, Tomasz Barszcz, Marcin Strączkiewicz, Adam Jablonski, Normalization of vibration signals generated under highly varying speed and load with application to signal separation, Mech. Syst. Signal Process. 82 (2017) 13–31.
[55] J.B. Allen, L.R. Rabiner, A unified approach for to short-time Fourrier analysis and synthesis, Proc. IEEE 65 (11) (1977).
[56] F. Combet, R. Zimroz, A new method for the estimation of the instantaneous speed relative fluctuation in a vibration signal based on the short time scale transform, Mech. Syst. Signal Process. 23 (2009) 1382–1397.
[57] A. Jabłoński, T. Barszcz, M. Bielecka, P. Breuhaus, Modeling of probability distributionfunctions for automatic threshold calculation in condition, Monitor. Syst. Measure. 46 (1) (2013) 727–738.
[58] J. Antoni, F. Bonnardot, A. Raad, M. El Badaoui, Cyclostationary modelling of rotating machine vibration signals, Mech. Syst. Sig. Process. 18 (2004) 1285–1314.
[59] D'Elia G., Daher Z., Antoni J., A novel approach for the cyclo-nonstationary analysis of speed varying signals. Proceedings of ISMA 2010 Including USD 2010
[60] J. Roussel, M. Haritopoulos, E. Sekko, C. Capdessus, J. Antoni, Application of Speed Transform to the Diagnosis of a Roller Bearing in Variable Speed, Proceeding of the conference Surveillance 7, France, October 29-30, 2013